High-Resolution Spatial Light Modulation for Holographic Video
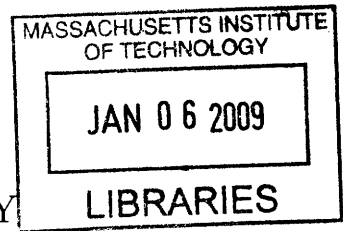
by

Daniel E. Smalley

Submitted to the Program in Media Arts and Sciences
in partial fulfillment of the requirements for the degree of

Master of Science in Media Technology

at the

MASSACHUSETTS INSTITUTE OF TECHNOLOGY

September 2008

Author . . . .
Program in Media Arts and Sciences
August 8, 2008

Certified by. . . . .
Dr. V. Michael Bove
Principal Research Scientist
Thesis Supervisor

Accepted by . . . .
Dr. Deb Roy
Chairman, Media Arts and Sciences Committee

High-Resolution Spatial Light Modulation for Holographic Video

by

Daniel E. Smalley

Submitted to the Program in Media Arts and Sciences
on August 8, 2008, in partial fulfillment of the
requirements for the degree of
Master of Science in Media Technology

Abstract

The goal of the proposed research is to further the fabrication of a high-bandwidth two-axis scanning device. The device is intended for use in a holographic video geometry built specifically to take advantage of the new modulator's high-bandwidth and vertical-deflection capabilities, but it could also be used in many developing 3D display systems which currently require high-bandwidth light modulation. The modulator will have a spatial frequency bandwidth one order-of-magnitude greater than current light modulation technologies and be two orders of magnitude less expensive.

Thesis Supervisor: Dr. V. Michael Bove
Title: Principal Research Scientist

High-Resolution Spatial Light Modulation for Holographic Video

by

Daniel E. Smalley

The following person served as a reader for this thesis:

Thesis Reader ....

Dr. Edward S. Boyden
Associate Professor
MIT Media Laboratory

High-Resolution Spatial Light Modulation for Holographic Video

by

Daniel E. Smalley

The following person served as a reader for this thesis:

Thesis Reader ...

Dr. Scott R. Manalis

Associate Professor

Department of Biological Engineering

Acknowledgments

My sincere thanks to:

- Dr. Bove, for the constancy of his support and encouragement.

- Quinn Smithwick, for taking on so much of the heavy lifting, mentally and physically, in the Mark III project.

- All the folks at NSL, MTL and SEBL, who gave me access to their facilities and valuable fabrication advice.

- Ed Boyden, Scott Manalis and George Barbastathis for their comments and suggestions.

- Neil Gershenfeld and his graduate students for allowing me to use their RF test equipment.

- The research presented in this thesis has been supported by the Digital Life, CELab, and Things That Think consortia at the MIT Media Laboratory.

Biographical Tidbit
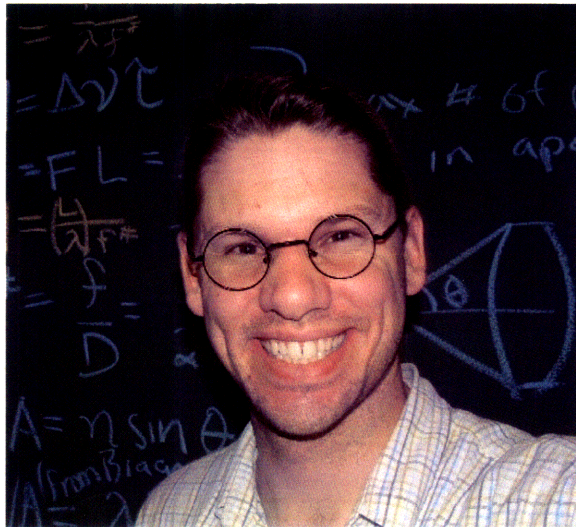
Daniel Smalley began experimenting with holography as a middle-school student living in rural Utah. After high school he began a correspondence with Elroy Pearson, then Research Assistant at the MIT Media Lab's Spatial Imaging Group, that led to his being invited to intern at the lab for the summer. During that internship he became familiar with the Mark II holographic video display, and with Dr. V. Michael Bove of the Object Based Media Group who participated in the creation of the Mark II. As a result of his experiences with Elroy and Dr. Bove at the Media Lab, he became resolved to create his own holovideo device, which desire became the impetus for a variety of related endeavors both at MIT and abroad including his current work with high-bandwidth modulators.

For Pamela, Neal and Jeffrey

Contents

List of Figures

List of Tables

Chapter 1

Introduction

1.1   Why 3D?

Much of the information in the world that we are interested in visualizing is three-dimensional, from MRI data to air traffic models to 3D animated games and movies. Furthermore, our human visual system is optimized to receive and process three-dimensional data. It is unfortunate[1], therefore, that most visualization is done using two-dimensional displays which create a bottleneck between our eyes and the world's vast and rapidly growing trove of 3D information.
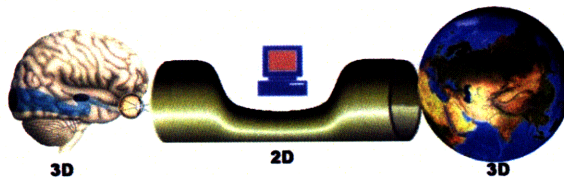
Figure 1-1: Two-dimensional displays have imposed a bottleneck between the richness of the world's abundant three-dimensional information and our own human visual system which is optimized for three-dimensional viewing.

---

[1]I have chosen to forward the argument that bandwidth is the key advantage of three-dimensional display instead of realism because the current state-of-the-art three-dimensional models rendered on flat screens are so compelling that some have argued that the increased realism provided by a three-dimensional displays might be marginal in many circumstances. This is, of course, an open debate. The assertion that three-dimensional displays provide greater visualization bandwidth is a more quantitative argument and more difficult to refute.

Display Type	Stereoscopy	Parallax	Accommodation	Occlusion
Discretized View Zone	●	●		●
Volumetric	●	●	●	
Holographic	●	●	●	●

Table 1.1: Three-dimensional displays and their respective depth cues.

1.2 Why Holographic Video?

Holographic video is potentially superior to all other 3D display techniques (stereoscopic, lenticular, volumetric, etc.) This is because holographic images can be made to possess all the depth cues important to depth perception[17], including those of accommodation and occlusion. Now if there existed a Consumer Reports article on buying 3D displays, it would probably contain a comparison like the one shown in Table 2.1, which summarizes the three-dimensional display categories and their associated depth cues[2].

When depth cues are missing in a three dimensional image, a viewer may experience eye fatigue, nausea or may not perceive depth at all. For these reasons, displays, like holographic displays, which contain all the requisite depth cues must be developed if three-dimensional displays are to be commercialized successfully in domains where two-dimensional displays are used today.

---

[2]In most cases, one type of display can be made to emulate another and, in so doing, will inherit that display's advantages and disadvantages. Discretized view zone displays, in the limit of many views (e.g. sufficiently many views to provide the eye with more than one view simultaneously), can begin to approach holographic displays. In the dense-view limit, the differences that remain between holographic and discretized-view zone are subtle, and typically involve discussions of coherent versus non-coherent illumination and point-spread functions. (In the coherent case discretized-view zone displays approach holographic displays in the same way an infinite sum of plane waves can be combined to create a point in space.) A discretized view or multi-view display in this dense-view regime inherits the ability to provide accommodation but also incurs the huge bandwidth requirement that is typical of holographic displays. Similarly, volumetric display hardware has been used to create a discretized-view display[16] and volumetric displays that match a holographic display's ability to reprduce all depth cues are possible. Consider, as has been suggested[16], a volumetric display made of a plane of pixels with each pixel capable of sending a different amplitude ray at any angle. This kind of display would not only be recreating the wavefront of an object, but would in fact be recreating a copy of the object itself– built time sequentially out of carefully controlled luminous points–a remarkable concept that not only inherits the bandwidth issues of holography but adds the complication of spinning everything at 30 frames a second. Of course, this type of luminous object reconstruction is only possible within the swept volume. Images may be made to appear outside the volume but only by means of discretized view zone techniques subject to discretized view zone limitations.

1.3 What has been done?

Almost any display can be a holographic display, so long as it possesses what I will call "holographic resolution." Holographic resolution is the pixel density required to diffract light over an appropriate viewing angle. I will arbitrarily choose 10 degrees as a minimum viewing angle which corresponds roughly to a pixel pitch of 1000 pixels per *millimeter* which, in turn, corresponds to a pixel size of one micron. This is the entire linear resolution of a modern computer monitor squashed into a millimeter length. It is this high resolution requirement that makes the practical implementation of holographic displays difficult.

Most of the current attempts at creating holographic displays are based on light modulators from existing two-dimensional display technologies like LCD[5], LCoS[14] and DMD[12]. The smallest pixel size achievable with these technologies is about 10 microns[3], so it is necessary to optically 'squash' and stack pixels to achieve holographic resolution. In all such displays to date this squashing and stacking has proven to be both difficult and expensive. To be fair, it is not really the fault of the LCD, LCoS or DMD devices that they are not perfectly suited for this application as they were made with two-dimensional displays in mind, three-dimensional displays were only an afterthought. It would be nice if someone were to come up with a light modulator specifically for three-dimensional imaging, perhaps something that started out with holographic resolution, so that squashing and stacking would be either easier to accomplish or entirely unnecessary.

1.4 My Contribution: The Wideband Guided-wave Optical Scanner

I am currently fabricating a spatial light modulator which possesses holographic resolution. The aperture of the device is small so that some stacking or scanning is

---

[3]This estimate was given in a private communication to me by Dr. Takeshi Honda of NEC corp. who has over 20 years of experience in the field of TFT displays.

Guided-Wave Scanner
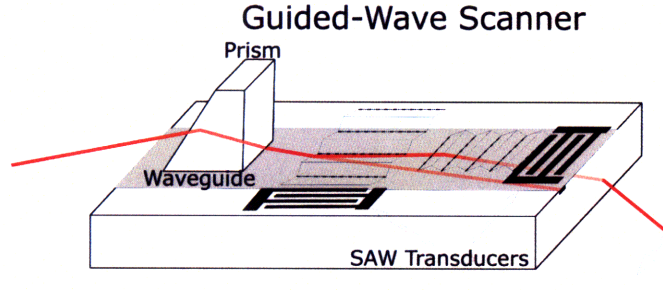
Figure 1-2: 2D Scanner

still required, but the device has been engineered with functionalities that make this scanning much easier than it would otherwise be. When completed, the device will be capable of producing a pixel pattern of greater than 1000 lines/mm at a rate greater than 1000MHz or a billion pixels per second[4]!

Primitive versions of the 2D guided-wave scanner fabricated with low-bandwidths were first created by Proklov[19] and later by Tsai[28] for use as proof-of-concept devices looking forward to possible application in fully-integrated spectrum analyzers. Tsai had also demonstrated high bandwidth (680 lines/mm or 680Mhz) 1D modulators and postulated that higher bandwidth 1D modulators were possible up to 1000MHz or 1000 lines/mm. This work seeks to realize Tsai's postulate for 1D scanners and go even further to apply the associated principles, for the first time, within a 2D scanner.

The scanner can be thought of as the combination of a fiber optic cable with a surface acoustic wave filter. In operation, laser light is coupled into a waveguide which is straddled by transducers. The transducers create surface accoustic waves

---

4

Notice the rather convenient fact that the lines/mm is roughly equivalent to the frequency bandwith in MHz. This is due to the fact that the speed of sound in Lithium Niobate is roughly 4km/s. So

$$\Lambda_{min}\Delta f = v$$

$$\Lambda_{min} = 4 * \mu m/line$$

$$\Delta f(Hz) \approx \frac{4000m/s}{4\mu m/line(.001mm/\mu m)}$$

$$\Delta f(MHz) \approx \frac{lines}{mm}$$

For the rest of this work well leave off the tilda and just assume that they are equal.

Wavguide   SAW Filter   Guided-Wave Scanner
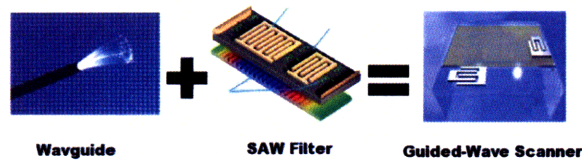
Figure 1-3: The 2D Scanner combines the function of fiber optics and SAW filter technology.

which diffract light horizontally in the plane (Fig. 1-4) and then vertically out of the plane (Fig. 1-5) resulting in a two dimensional scan. The second interaction is polarization rotating so that undiffracted light and other noise can be effectively removed with polarizers. The fabrication process itself is simple (by comparison with semiconductor devices), requiring only two masks so that, when fabricated in quantity, the devices can be made for only a few dollars each.

Horizontal Scan
Bragg diffraction
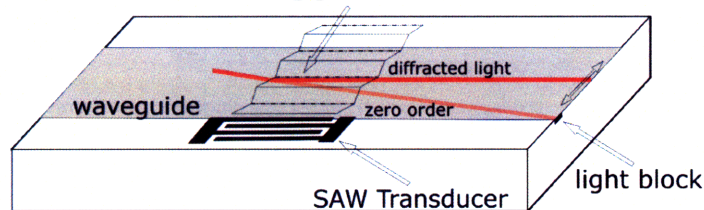
Figure 1-4: Non-collinear, in-guide diffraction

Vertical Scan
Mode Coupling
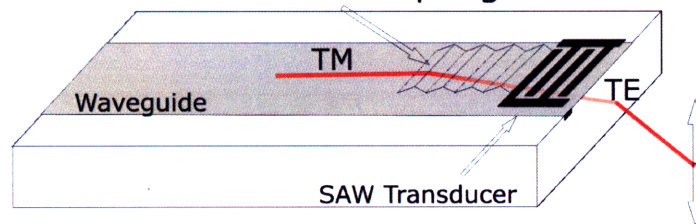
Figure 1-5: Collinear out-of-guide TM-TE mode coupling

The scanner will be used as part of the third generation MIT Holovideo Display,

called Mark III (Fig.1-6). The Mark III optical geometry, which has already been constructed by Dr. Quinn Smithwick, has been designed to leverage the scanner's unique capabilities. For example, the scanner's vertical deflection is used in conjunction with a holographic element to de-rotate the holographic diffraction pattern as it travels across the scanner, this interaction accomplishes the scanning and stacking that was mentioned earlier but without the use of fast horizontal scanning mirrors as was the case for previous MIT holovideo prototypes. With the elimination of the fast scanning mirrors and the introduction of the guided wave scanner as the light modulator, the display's cost is reduced by two-orders of magnitude. Dr. Bove has articulated the goal of using this new geometry to create a display that is, "'the size and cost of a CRT monitor."[22]

Simplified drawing of the Mark III holographic video display
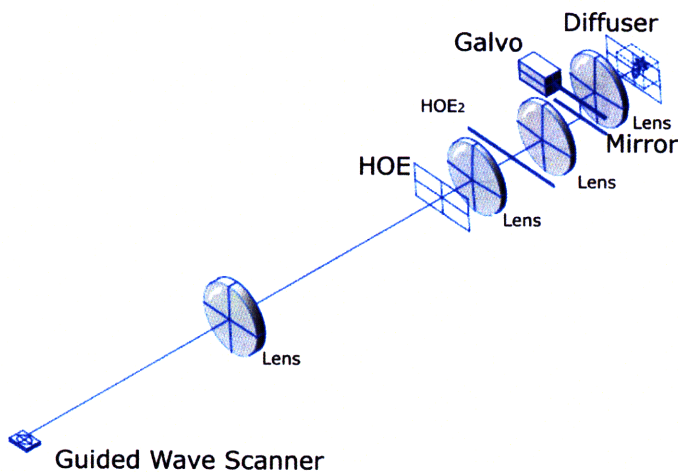
Figure 1-6: The Mark III optical geometry (Courtesy of Quinn Smithwick).

1.5 Problem Definition/Approach

The goal of this work is to complete the fabrication of the guided wave scanner.

A completed scanner is capable of coupling, confining, diffracting and mode converting light. Furthermore, the scanner will be able to cascade the Bragg diffraction and mode-conversion steps and have optimized waveguide and transducer parameters

so as to maximize diffraction efficiency and mode-coupling bandwidth.

1.5.1 Desired Capabilities

The desired capabilities for the scanner are:

- 1 Ghz RF transducer bandwidth (which corresponds spatially to holographic resolution of 1000 lines/mm)

- 10% or greater diffraction efficiency

- aperture of 1mm or greater

1.6 Evaluation

This research will be considered sucessful to the degree that the final fabricated scanner meets the desired capabilities of high resolution, high diffraction efficiency and wide aperture mentioned above.

1.7 Summary

With the creation of a working guided wave scanner, the world will have a light modulator that is better matched to the needs of three-dimensional display than any that it has seen to date. Furthermore, the low cost of the scanner and the supporting holovideo geometry will make it possible for holovideo to be used by more people in more ways than ever before.

Chapter 2

Background

2.1 Holograms are simple
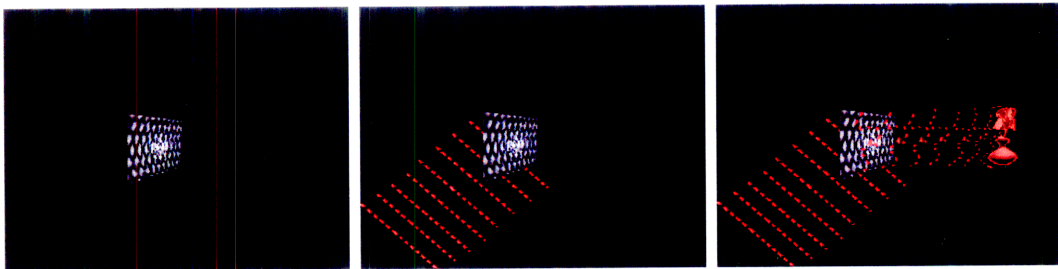
Figure 2-1: A hologram reproducing a light field

A hologram is really just a high resolution pattern that modulates either the amplitude or the phase of light. Such loose restrictions have made it possible to create holograms of all sizes in all sorts of media. Life-sized holographic portraits have been produced. Holograms have been made optically on film, embossed on foil, and written in oil with electron beams. Holograms have even been pressed into chocolate!

2.2 Holovideo displays are complex

Electroholographic displays tend to be as complex as static holograms are simple (see the Mark II geometry, constructed by Pierre St.-Hilaire[25], shown in Fig. 2-2). The
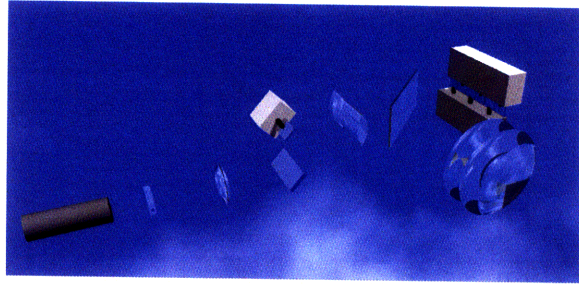
Figure 2-2: The Mark II optical geometry

reason for this is that it is very difficult to make a dynamic light modulator, phase or amplitude, that's as *dense* (e.g. densely patterned) and as *big* as a typical film hologram.[1]

2.2.1 Denser? Demagnify!
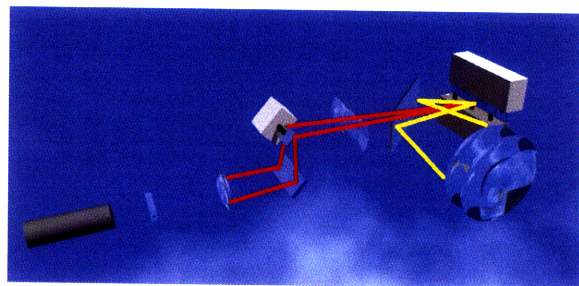
Figure 2-3: Highlighted, is the telescope system responsible for demagnification in the Mark II geometry

The first contributor to complexity in holographic displays is the need to make them dense, that is, to have high spatial resolution. The higher the spatial resolution, the higher the angular diffraction and the wider the view zone of the resulting display. Since the desired minimum feature of our hologram is approximately 1 micron and the smallest feature easily achievable with DMD's, LCD or LCoS technology is around

[1]When it is possible to make such modulators [3], updating at video rates proves to be daunting. An example of this is the remarkable, updatable holographic display created by researchers at the University of Arizona (a team with includes Mark II pioneer Dr. St. Hilaire) who have made what is essentially a rewritable holographic film. The complication then is shifted to the writing device which, for video-rate updates, would likely be a device like the modulators described above, and subject to the same limitations. Additional examples would be the QinetiQ display[5], T.C. Poon's ebeam written displays [18] in which an OASLM front end is written with an electronically addressed spatial light modulator or an electron beam respectively. In all these cases the light modulator presents a bandwidth bottleneck.

10 microns, we typically need to de-magnify, using a four-f lens system, the light modulator pattern by a factor of ten. This usually means that a holographic system will need a telescope system of two lenses, where one lens is relatively powerful (the Mark II uses an output lens with an f-number near 1). The telescope system in Mark II is highlighted in Fig. 2-3. Of course, now we have a pattern that diffracts well angularly, but it's ten times smaller that it was initially which means we'll have to scan or stack (multiplex) the modulator's output to build up an output that is of useful size.

2.2.2 Bigger? Descan!
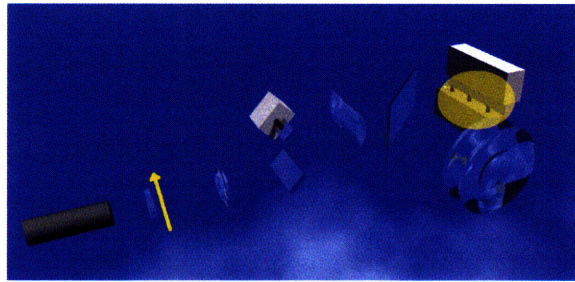
Figure 2-4: Highlighted, is the bank of horizontal scanning mirrors responsible for ing:ing the holographic image in the Mark II geometry

The Mark II's modulator is already scanning, so it uses a bank of scanning mirrors (highlighted in Fig. 2-7) to de-scan or de-rotate the modulator's holographic pattern so that it appears stationary. The process of descanning is illustrated in 2-5. A vertical mirror scans horizontal lines to produce the final output.

| | | |
| (a) | (b) | (c) |
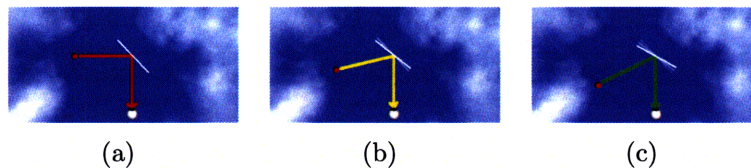
Figure 2-5: Descanning: as the ball moves the mirror rotates to keeps the ball's image stationary

(a) QinetiQ[5] (b) SeeReal[11] (c) Hyogo[26] (d) Texas[12]
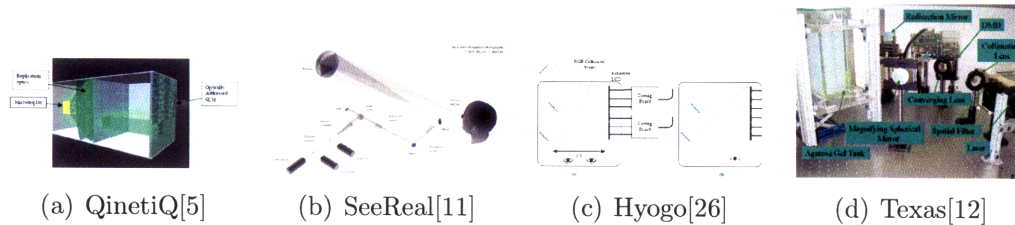
Figure 2-6: Examples of Holographic Displays

Display Type	Modulator	Approx Pixel Size	Angle by:	Size by:
QinetiQ	EASLM	10-20 μm	lens system	shutter/lens system
Mark II	AOM	6 μm	lens system	scanning mirrors
SeeReal	LCD	25 μm	none	Eye Tracking
Hyogo	LCD	8.1 μm	multiple modulators	multiple modulators
Texas	DMD	16 μm	Diffuser	lens/diffuser

Table 2.1: A summary of holographic displays, their modulators and their approaches to achieving adequate size and view angle

2.2.3   Other Displays

Just as with the Mark II team[25], everyone building holographic displays has had to grapple with the problem of achieving adequate view angle and size with light modulators that are too low resolution to serve as holograms directly. Their approaches vary widely, and many are impressive, but in all cases the resulting geometry is relatively complex and expensive.

QinetiQ Display, 2004

QinetiQ has developed a display that tiles the output of a fast 1Ghz bandwidth Electrically Addressed Spatial Light Modulator (EASLM) onto an Optically Addressed Spatial Light Modulator (OASLM)[5]. A shutter in front of a wall of lenses allows the display to write de-magnified images of the EASLM onto abutting regions at the OASLM. This display boasts modular design, full-parallax and full color.

SeeReal, 2008

The SeeReal[11] display doesn't demagnify its modulator, instead, it uses eye tracking to locate the viewers pupils, and steers the small-angle diffracted output of its large

LCD panel to fill in only those portions of the light field that are entering the viewer's eyes.

Hyogo, 2005

Atsuhiko Sugita and his collegues at Hyogo University have used six reflective LCD's to achieve either wide viewing angle (21°) and small display (15.5mm wide) or large display (93mm wide) and small viewing angle (3.5°)[26].

Texas, 2004

Bala Munjuluri and his colleagues at the University of Texas, use a Digital Mirror Device (DMD) as a dynamic holographic grating[12]. This means that the display has a relatively low bandwidth requirement and a low-cost, straight-forward design. However, the low bandwidth means low diffraction angle, so the output of the display is projected into an omni-directional diffuser that is meant to widen the angle of view, but also has the effect of turning this display's holographic points into volumetric points!

The displays discussed above use varying techniques from shutter/lens demagnification to eyetracking. The displays mentioned above with outputs that are closest to that of a typical hologram, in size and view angle, are the most complex and the most expensive (a conservative estimate would put the price of the QinetiQ display at over one hundred thousand dollars).

2.3   Problem: Low Bandwidth Modulators

So why are holograms so simple and holovideo displays so complex (and expensive)? The reason is because commonly available modulators are small and not of sufficiently high resolution to effectively act as holograms. Said in other words, they don't have a sufficiently high space-bandwidth product. We might be able to live with a small modulator (making a big lens might be easier than making a big modulator) so the 'space part' of the space-bandwidth product is negotiable, but getting as high a
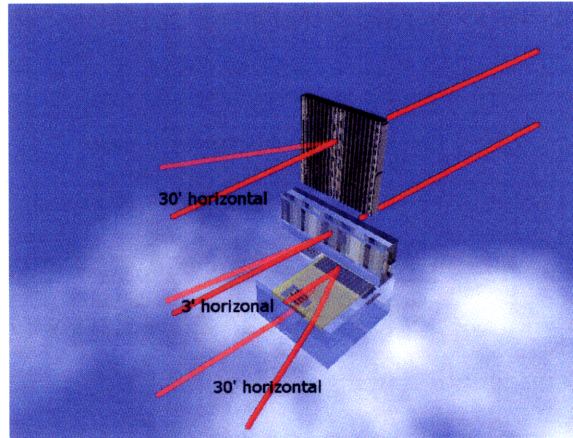
Figure 2-7: The hologram (top) has high spatial resolution and can therefore diffract over large angles. The AOM (middle) and other modulators like DMDs and LCDs have a spatial resolution that is approximately ten times smaller than a typical hologram and their ability to diffract is proportionally lower. One of the goals of my work with the Guided Wave Scanner (bottom) is to create a modulator with a spatial frequency on the order of a typical hologram, capable of equivalently large angles of diffraction.

bandwidth as possible is an absolute necessity. For LCDs, this means making smaller pixels, but since the thickness of the nematic cell is fixed, the resulting aspect ratio for each pixel becomes difficult to achieve by standard photolithography. For both DMDs and LCDs, scaling down the pixel would also mean scaling down active backplanes which would bring additional complexity into the fabrication of the modulator. For AOMs (Acousto-Optic Modulators), higher resolution is relatively easy to achieve, one need only use a higher bandwidth crystalline material (one that doesn't attenuate at ultrahigh frequencies). The problem with high bandwidth AOMs, however, is that you must find a way to descan your acoustic pattern that may be travelling at several kilometers a second! The Mark II accomplishes this by using a bank of fast scanning galvos and by employing a bulk wave AOM with a slow-shear mode of approximately 600m/s. Unfortunately, the AOM material, TeO_2 has significant acoustic attenuation for drive signals above 100MHz which limits the effective pixel size to $6\mu m$. Lithium Niobate has a much higher bandwidth, allowing drive signals up to 20GHz, but it has an acoustic velocity of approximately 4km/s–which is far faster than the Mark II galvos could hope to descan.

2.4   Solution: the Guided Wave Scanner

Guided-Wave Scanner
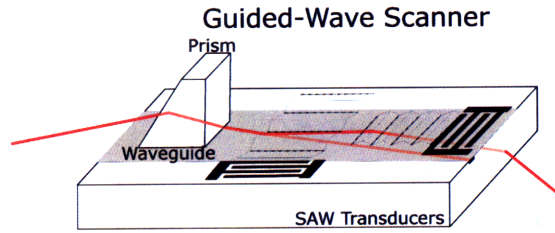
Figure 2-8: The Guided Wave Scanner

The high Bandwidth modulator described in this thesis is a Lithium Niobate AOM which deflects light trapped in a waveguide with Surface Acoustic Waves (SAWs). Light is deflected horizontally by Bragg diffraction and then vertically via guided-to-leaky mode conversion. The problem of bandwidth is solved by virtue of the fact that Lithium Niobate is a high bandwidth material. The problem of descanning the fast-moving acoustic signal is solved by using the vertical scan coupled with a special holographic optical element(HOE) to descan the pattern without the use of moving mirrors.

The HOE is capable of converting vertically scanned light into horizontally scanned light in a horizontal parallax only (HPO) system. A more complete treatment of the HOE is given in the appendix.

2.4.1   Previous work

Primitive versions of the guided-wave scanner were first created by Proklov[19] and later by Tsai[28] for use as fully-integrated spectrum analyzers.

A discrete descan system, similar to the one shown here, was made part of a pulsed holographic display by Son et al.[24].

The new modulator and HOE will become part of the Mark III holographic video display. The Mark III is an improvement on the Mark II in that the horizontal bank of scanning mirrors is replaced in this generation by a holographic optical element (HOE), rendering the horizontal de-scan entirely solid-state. Additionally, the more expensive bulk-wave modulators will be replaced by the inexpensive guided wave

device. Finally, Quinn Smithwick has designed this geometry using all stock lenses and provided for the possbility for folding the geometry into a container the size of a CRT.

Simplified drawing of the Mark III holographic video display
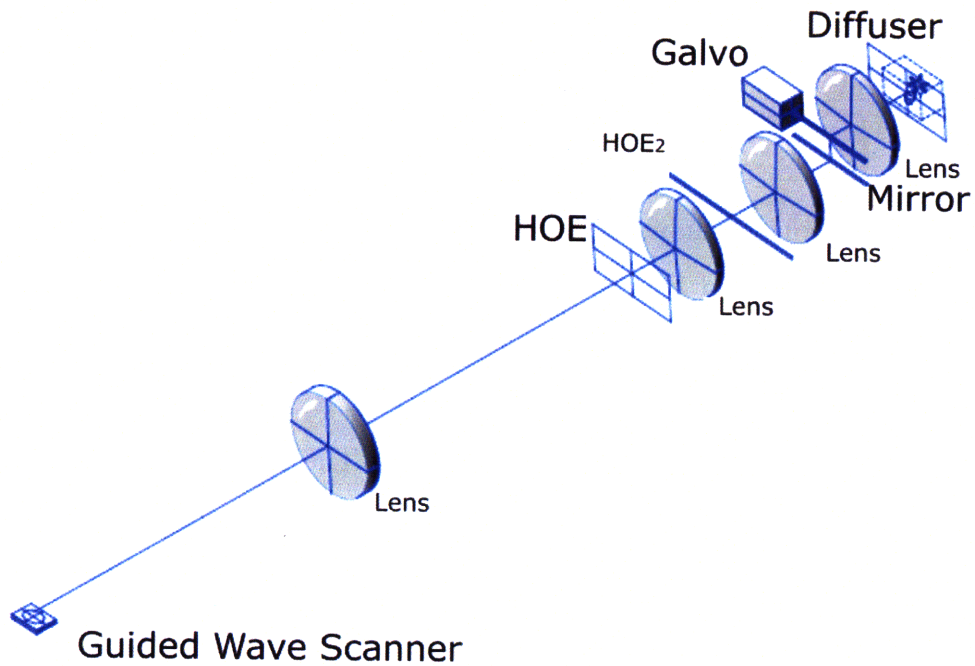
Figure 2-9: The Mark III Holovideo Geometry (Courtesy of Quinn Smithwick)

Chapter 3

Theory

This chapter gives a brief description of the phenomena involved in the 2D scanner's function[1].

3.1   Relevant Literature

Many of the papers most relevant to the function and design of the guided-wave scanner are found in the book "Guided-Wave Acousto-Optics" edited by Tsai[29] [28] though the device appears in its rudimentary form in early works [19]. Tsai's book describes in some detail the design of waveguides and transducers (both simple and phased) for use in guided wave devices.

The literature most relevant to the holographic video geometry includes Dr. St.-Hilaire's PhD Thesis on the Mark II system, [25] and those theses that predate his work [7],[10].

3.2   The Guided Wave Scanner

Five important things are happening in the guided wave 2D scanner: coupling, confinement, surface acoustic wave generation, Bragg diffraction and mode conversion.

---

[1]This chapter has been adapted, with some minor changes, from my previous thesis.[21]

3.2.1 Coupling

Laser light enters the scanner's waveguide through evanescent coupling. A right angle prism of high refractive index material (rutile or indium phosphide) sits on top of the waveguide and is pressed until a 'wet spot' appears indicating that there is close contact between the prism and the substrate (even with good contact, there is typically some air gap.) Light focused just below the 90-degree corner enters the crystal and reflects off its bottom and side faces, back towards the laser source. At the bottom of the prism, evanescent fields extend through the air gap and into the waveguide. The angle of the light entering the prism is adjusted and as it varies the spatial frequency of the light at the boundary of the prism/gap interface changes. This spatial frequency at the boundary is called the propagation constant or the wavenumber, β. The waveguide only allows for the propagation of certain wavenumbers called 'modes'. When the laser is tilted to the correct angle, the evanescent fields couple light into the waveguide where it travels as a mode. Prism coupling efficiencies of 81% or more have been reported[27], but efficiencies of 30-50% are more common in practice. It is also possible, though more difficult, to couple light into the waveguide through an etched diffraction grating on the surface, or by butt-coupling a laser or lens tipped fiber to the edge of the guide. These methods are more economical and better suited for mass-production, but for experimentation, prism coupling is more convenient.

3.2.2 Confinement

The waveguide is formed by 'proton exchanging' the surface of Lithium Niobate. Proton exchange is performed by immersing the Lithium Niobate wafer in a melt of Benzoic Acid. The exchange turns $LiNbO_3$ into $HNbO_3$ which has a much higher extraordinary index of refraction $\Delta n_e = +0.12$ (from $n_e = 2.2028$ to $n_e = 2.3278$) and a slightly lower ordinary index of refraction $\Delta n_o = -0.04$ [30] (from $n_o = 2.2860$ to $n_o = 2.2460$). Light can be index guided whenever a high index material is surrounded by two materials of lower index of refraction. $HNbO_3$ is surrounded on top by air with an index $n = 1$ and on the bottom by $LiNbO_3$ with an index $n_e = 2.2028$ so TM

light is guided in the proton exchanged layer, but TE polarized light is not.[2]

3.2.3   Surface Acoustic Wave Generation

Surface acoustic waves are generated by interdigital transducers through the piezo-electric effect and are subject to various loss mechanisms related both to the IDTs (impedance matching) and to the nature of SAW propagation itself.

Interdigital Transducers (IDT's)

In order to create surface acoustic waves, an interdigital transducer is fabricated on top of Lithium Niobate. When voltage is placed across the electrode fingers, the piezoelectric effect gives rise to stress and strain in the crystal. When the voltage is relaxed, the mechanical energy is released as Rayleigh waves that travel on the surface of the crystal like ripples on water. The interdigital transducer is made of several finger pairs. Each finger pair acts like a point or line source for surface acoustic waves. When several of these finger pairs are placed next to each other, they act like an end-fire antenna array, launching waves only out of the two ends of the transducer. The transducer's center frequency is determined by the electrode period and the bandwidth is a function of the number of finger pairs. Both dependencies are governed by the following relations:

$$f = \frac{v}{2p} \tag{3.1}$$

$$B \approx \frac{1}{N} \tag{3.2}$$

where f is the center frequency, v is the velocity of sound in Lithium Niobate, p is the period defined as one half the acoustic wavelength, B is the fractional bandwidth (bandwidth/center frequency) and N is the number of finger pairs.

---

[2]Please note that we are using the engineer's definition of TM/TE polarization and not the mathematician's definition. To be explicit, the transverse field is that field which is transverse to the plane made by the incident and reflected/refracted rays of light.

Also, electrical to SAW power coupling efficiency goes up with the number of finger pairs, n. This results in a tradeoff between large bandwidth and high coupling efficiency. [3]

Impedance Matching

The interdigital transducer has a complex impedance exhibiting real resistance and imaginary reactance. The transducer is impedance matched when a series inductor is used to cancel the capacitive reactance. If the real resistance is not 50Ω after the inductor is added, a second matching element can be used to bring the total real resistance to 50Ω. The real resistance can be thought of as proportional to the width of the transducer, with shorter transducers having a larger resistance than longer transducers. The goal is to design a transducer that can be matched with a single inductor to a real resistance of 50Ω. We can design such a transducer when we understand which mechanisms give rise to loss in the transducer. In a SAW filter, the real resistance has two components: an ohmic resistance, R_{ohmic}, and a radiation resistance R_{rad}. The matching inductor may add some ohmic resistance but this is often small. The value given for the radiation resistance is a closed form equation derived from an equivalent circuit model for the SAW transducer by Reeder[29].

$$R_{rad} = \frac{4k_c^2}{\pi\omega_0 C_g^* W} \tag{3.3}$$

where k_c^2 is the coupling coefficient, ω_0, the angular center frequency, C_g^*, linear capacitance density and W, the SAW acoustic aperture. The ohmic resistance is given as,

$$R_{ohmic} = \frac{4W R_s}{N\Lambda} \tag{3.4}$$

where R_s is the resistance per square, N is the number of finger pairs and Λ is the acoustic wavelength.

For non-uniform transducers, like slanted or chirped transducers, there are matrix

---

[3]Complex transducers involving chirped periods, or slanted fingers are not limited by the bandwidth relation above and can be made to have both wide bandwidth and a large number of finger pairs for efficient wideband operation.

methods[23][6][20] for determining the radiation resistance. These transducers may be used in future iteration of the guided-wave optical scanner.

In order to design a transducer to be 50Ω when matched, we set the sum of R_{ohmic} and R_{rad} to 50Ω and backsolve for the appropriate width, W. Unfortunately, as frequency goes up the corresponding W for a 50Ω design goes down and so the diffraction efficiency of the SAW wave produced decreases since the aperture width is the interaction length for diffraction. Tsai proposes an alternate, more sophisticated, design for high frequency transducers that involves a phased array of 50Ω transducers capable of beam steering with frequency to meet the Bragg angle for large range of frequencies while maintaining a large effective width[29]. Phased transducers have not been investigated thoroughly in this work, but we will likely have to use this approach for the higher frequency transducers when getting a uniform output becomes the chief concern. For the present investigation all transducers have been kept simple and uniform.

Loss Mechanisms

The Rayleigh waves should, ideally, propagate without loss on the crystal surface, but, likely because of viscous damping, there is a frequency-dependent attenuation of propagating SAW waves. Lithium Niobate, however, attenuates acoustic waves at a much lower rate than does Tellurium Dioxide (Tellurium Dioxide, as readers will recall, was used in the AOM for Mark II). For Lithium Niobate the attenuation can be expressed as :

$$Attenuation(dB/\mu s) = 0.88F^{1.9} + 0.19F$$

[2] where F is frequency in gigahertz. For 500MHz, the attenuation is 0.33dB/μs. Contrast this with the acoustic attenuation for Tellurium Dioxide (TeO$_2$): 3dB/μs @ 500MHz for slow shear mode. More impressive still is the fact that because the wavespeed of the slow shear mode in Tellurium Dioxide is 617m/s, acoustic waves in TeO$_2$ will be attenuated by 3db after only 0.6mm of propagation while SAW waves in Lithium Niobate, traveling at 3909m/s will not be attenuated by 3db until they have

traveled over 39mm for frequencies near 500mHz. Lower attenuation means that it is possible to create displays with larger optical apertures which have greater available image depth.

Additional sources of loss include insertion loss and acoustic diffraction. Insertion loss tends to increase with frequency while acoustic diffraction goes up as the electrode length is reduced (as the effective aperture gets smaller). Diffraction loss may be ameliorated by adjusting the overlap (apodization) of each finger pair to modify the far-field SAW mode pattern. One can eliminate SAW diffraction due to the width of the transducer by apodizing a sinc function (the Fourier transform of the desired far field SAW pattern) along the length of the transducer. Surface acoustic waves generated and filtered in this way by one transducer may be subsequently filtered again and absorbed by a second transducer making very flexible and efficient passive filters[15] and optical modulators.

3.2.4 Isotropic Bragg Diffraction

SAW waves are made of regions of compression and rarefaction which are capable of two types of diffraction: Raman-Nath (thin-film) diffraction or Bragg (thick-film) diffraction. Raman-Nath diffraction occurs when the thickness parameter Q is much less than one[1].

$$Q = \frac{2\pi\lambda * t}{nd^2 \cos\theta_0} << 1$$

Q is the thickness parameter, t is length of the interaction region, d is the distance between fringes, n is the index of refraction and θ is the angle of incidence. In this regime light meets a brief interaction region made of apertures that diffract light to create multiple orders with a maximum first-order diffraction efficiency of approximately 40.5%[1] for thin binary phase gratings and less, 33.8%, for sinusoidal gratings as dictated by the fourier transform. In Bragg diffraction, light enters a longer interaction region of Bragg-planes where the light is both guided as well as diffracted when it meets the Bragg condition (which means it enters at the Bragg angle). This

44

guidance leads to constructive interference of one order and the distructive interference of all other orders resulting in a single order of diffracted light with a maximum efficiency of 100%. As an interaction region becomes longer, and as the resulting diffraction moves smoothly from Raman-Nath to Bragg, the diffraction efficiency becomes greater and the allowable input angle for light becomes tighter. The angle of incident light required for Bragg diffraction is called the Bragg angle.

$$\theta_b = \arcsin \frac{\lambda}{2d}$$

Lambda, λ is the wavelength of light and d is the distance between Bragg planes. I wish to be operating as much as possible in the Bragg diffraction regime so that I can take full advantage of the higher diffraction efficiency and single-order characteristic of this type of modulation. This means that I must design my transducers with as wide an aperture as is allowable without driving the transducer impedance too low.

Horizontal Array of Transducers

We wish to fabricate a scanner that can diffract light over a large range of angles; 10 degrees is an ambitious but reasonable goal for red light in the Mark III system[4]. 10 degrees of diffraction corresponds to an RF bandwidth of, using the Bragg equation:

$$\delta f = \frac{2v \sin 5deg}{\lambda} = 1.07 Ghz$$

(where λ=633nm and v=3909m/s)

We need a transducer that has a bandwidth of 1Ghz. By using a simple uniform transducer with only a single pair of electrodes, $N = 1$, we can achieve the requisite bandwidth by placing the center frequency of the transducer at 1Ghz. The very low number of pairs and the very high center frequency make this an extremely inefficient transducer. Raising the center frequency to 2Ghz and doubling the number of pairs does not help much. We could use a slanted transducer or a chirped transducer, but

---

[4]I should note that, ultimately, the Mark III will be illuminated with a green laser at 532nm. The green laser will give more mW of light per dollar than a comparable red laser but the resulting diffraction will be smaller (in proportion to the reduction in wavelength).

that would add a lot more complexity and still would not be as efficient as using an array of simple transducers as suggested by Tsai[29]. In the end, I decided to break up the requisite bandwidth of 1Ghz into ten chunks, using a ten transducer array[5]. Each transducer must be tilted to meet a different Bragg angle.

The holographic information is fed into this array of transducers producing surface acoustic waves that cross the waveguide where laser light is traveling at the Bragg angle for each transducer. Note that light will diffract only once, because, once it has diffracted, it will no longer be traveling at the Bragg angle. Furthermore, the laser illumination angle is adjusted and the horizontal transducers slightly rotated so that diffracted spread of light output travels in the direction of the second collinear transducers where mode conversion of the newly diffracted light takes place.

3.2.5 Mode Conversion

The vertical scan is accomplished using collinear surface acoustic waves that convert the guided TM mode light into leaky mode TE polarized light. This collinear transducer has roughly a 460Mhz center frequency, a 50Mhz bandwidth and is similar to the transducers described above, but orthogonally rotated so that the output SAW waves are traveling along the length of the waveguide, 'head on' toward the incoming diffracted light spread. The collinear wave basically diffracts the light down, out of the waveguide and changes its polarization in the process. A slightly better way to think about this interaction is to say that the momentum vector of the acoustic wave is subtracted from the momentum of the diffracted light vector resulting in a light wave with a reduced wavenumber (propagation constant). As I mentioned earlier, waveguides only support light of particular wavenumbers, so if the wavenumber of guided light is changed, then it is no longer guided[6]. Instead, the light scatters, and

---

[5]The Mark II uses a dual-head graphics chip which provides six outputs of 200MHz bandwidth each. The most efficient transducer array designs distribute more bandwidth to higher frequency transducers and less bandwidth to lower frequency transducers. So the first graphics chip output will be split to the first three transducers (the three lowest in center frequency). Next, the second output will be split to the fourth and fifth transducers. Finally, the remaining four outputs will be paired with the last four transducers.

[6]Unless, of course, it is changed to a wavenumber corresponding to another other mode of the waveguide.

46

since it is scattering from a periodic structure (i.e. the SAW pattern), it has a favored direction and polarization which in this case is down into the substrate with TM polarization (all TE scattered light is trapped in the waveguide where it destructively interferes with itself and disappears). The most complete explanations require the use of a special case of Haus Coupled Mode Theory[4]. The upshot of this mode conversion is that, by varying the frequency on the collinear transducer I can scan the diffracted light vertically as it drops out of the waveguide and exits the crystal. This vertical deflection becomes an extra degree of freedom that I can use to perform the horizontal de-scan.

3.3   Mark III geometry

Let's review the system-level light path of the Mark III:

Laser light couples into the waveguide of the guided-wave scanner. SAW waves, acting as holographic fringes traveling *orthogonal* to the light in the 'y' direction, cross the guide and modulate the confined light through isotropic Bragg diffraction. Then SAW waves *collinear* to the diffracted light traveling in the 'x' direction rotate the light's polarization and diffract it down and out of one of the crystal's faces. Next, the light travels through a four-f processor with a de-scanning HOE at the Fourier plane. As the guided-wave scanner translates the light vertically, the HOE deflects horizontally so that when the light emerges from the four-f system its holographic information has been de-scanned and appears stationary. A second HOE collimates the light and passes it through a second four-f system, this time meeting a vertical scanning mirror at the Fourier plane and emerging multiplexed vertically to build a screen-sized output. Finally, the light travels through a vertical diffuser which creates a vertical focus in space while the light focuses horizontally into points forming a holographic image viewable by the observer.

3.4 System Assumptions

In using the guided-wave scanner and the HOE solution, we make the assumptions that sufficient light can be coupled into the device to produce display level brightness on the output. The output of the display is highly directional compared to other displays so the requirements for power are somewhat looser, however there is significant loss at the guided-wave device. There will be a considerable loss of light when it is coupled into the waveguide, and at least half the light will be lost at the horizontal diffraction step and another half will be lost during the collinear TM/TE coupling step. These losses by themselves should be tolerable, considering the fact that the noise is eliminated by polarizers. Care will need to be taken to reduce the total number of external interfaces and other diffractive losses in the HOEs adding to the total system loss.

It is also assumed that the change of frequency of the collinear interaction will be fast with respect to the angular change of the helical mirror so that only one effective angular view will be addressed at a time, otherwise a loss of views or overlapping of views may result. However, even if it does turn out that more vertical resolution is needed, the interaction length used by the vertical scan can be increased to add vertical resolution.

Chapter 4

Design of the Guided-Wave Scanner

The guided wave scanner is made in a very flexible fashion. There are a dozen or more methods of creating waveguides in Lithium Niobate and there are innumberable transducer configurations that one might use. This chapter details my design decisions for making a device suitable for wideband scanning and macro-scale display.
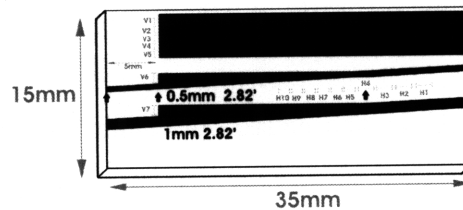
4.1 Waveguide Design

Figure 4-1: Waveguides in black

The first design decision to be made is which proton donor to use. I chose Benzoic Acid. Other promising donors exist (including Octanoic Acid, Phosphoric Acid and Sulfuric Acid) but none is as frequently reported in the literature as Benzoic Acid.

The next decision is which of all the variations of proton exchange (I can name ten) should be used. The most common are either pure-melt proton exchange (PE)

or Dilute-Melt Proton Exchange (DMPE). I decided against DMPE because, while it produces low-loss waveguides, diluting the melt leads to a reduction in the optical damage threshold of the guide as shown in the Fig4-2 from Miyawaki. Since I hope to use these devices for macro-scale display it seems to make sense to try to preserve the high power capacity of the waveguide.
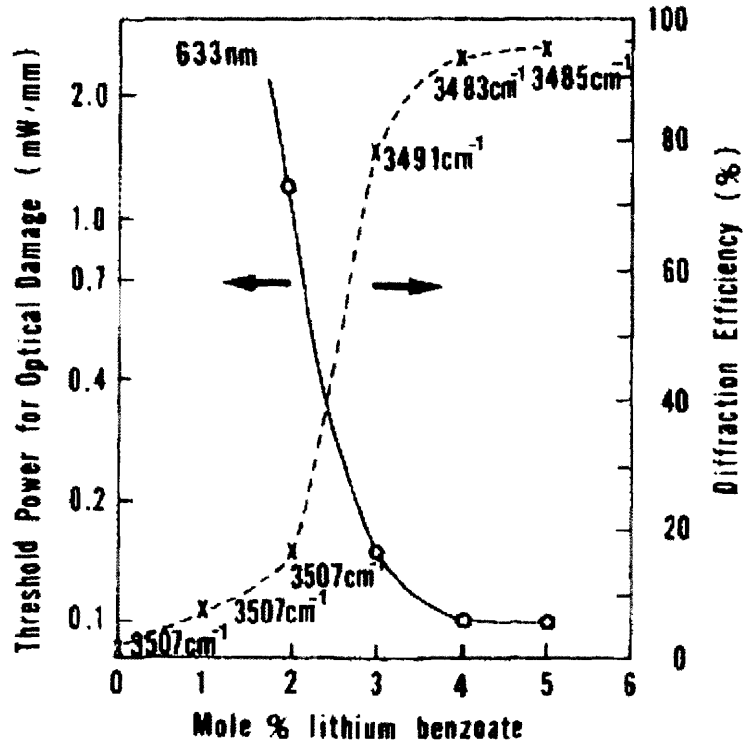

Figure 4-2: Optical damage threshold with melt dilution (from Miyawaki[13])

Pure-melt exchanges reduce the elasto-optic and piezo-electric properties of the Lithium Niobate substrate so it is necessary to anneal the waveguide after the exchange. Annealing diffuses the waveguide and reduces the confinement of the light and the overlap between light and soundwaves in the guide. To maximize the restoration of the substrates properties and minimize the diffusion of the waveguide, I refer to the following plots by Kakio (Fig.4-3 and Fig.4-4) to arrive at anneal time of approximately 45 minutes.

The waveguide depth will determine the mode number, separation and resultingly the mode coupling frequency and bandwidth. Matteo[4] performed a series of mode
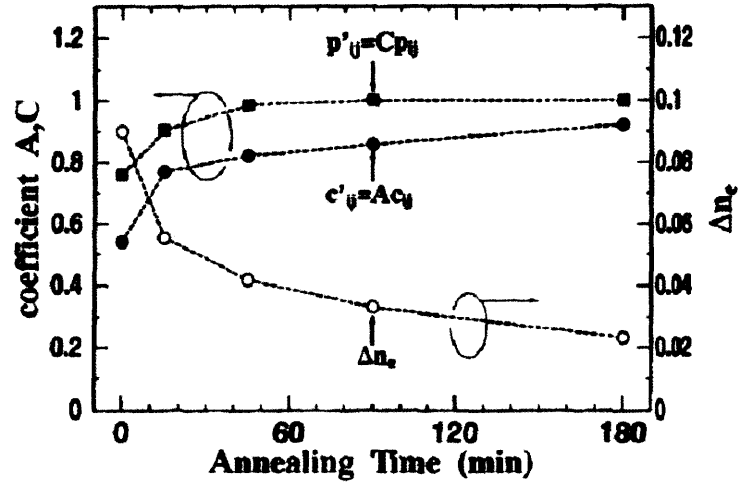
50

Fig. 6. p'_{ij}, c'_{ij} and Δn_e dependence on annealing time.

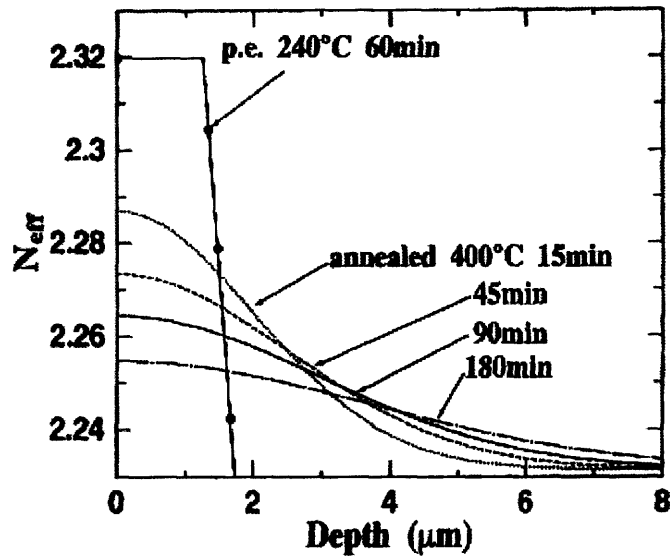Figure 4-3: Restoration of photoelastic constant with anneal time (from Kakio[9])

Figure 4-4: Alteration wavguide profile with anneal time (from Kakio[9])

coupling simulations for various cuts of Lithium Niobate. The Z-cut mode coupling spectrum is shown below in Fig. 4-5. For applications requiring large bandwidths, Matteo suggests using a waveguide depth of $1\mu m$ which, as can be seen below, has a mode coupling peak at 460MHz with a 60MHz bandwidth[1].
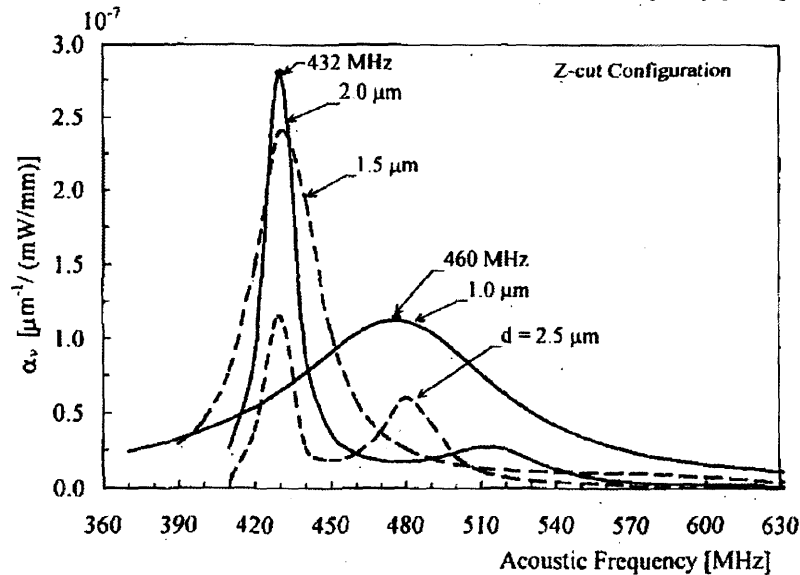

Figure 4-5: Mode coupling spectrum for different waveguide depths (from Matteo[4])

The literature has reported that PE waveguides have a step like profile and can be described using the following diffusion constants, $D = 0.44\mu m^2/hour$ for Z-cut Lithium Niobate at $236°C$ [8] and thickness, $\tau = \sqrt{4DT}$ where T is Temperature. At $236°C$ a $1\mu m$ deep waveguide requires a 30 minute exchange time.

4.2 Transducer Design

4.2.1 Parameter Interaction

There are a large number of parameter interactions to consider when approaching transducer design. A simplification of the parameter interaction is presented in Fig. 4-8, and an attempt to describe the most important parameter interactions is given below.

---

[1]Please note that this analysis does not take into account the effect of annealing, which may alter the mode-coupling behavior of waveguide.
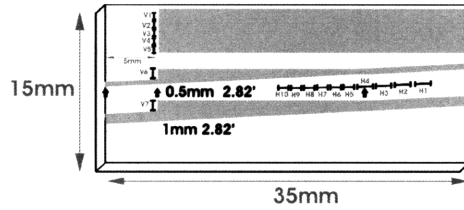
Figure 4-6: Transducers in black
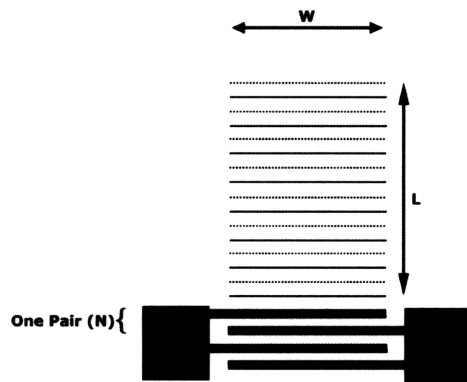
4.2.2 Parameter Interaction

Figure 4-7: Transducer parameters

The diffraction efficiency, η_{Bragg}, increases with higher induced index contrast, ΔN, greater interaction length, W, and a maximized overlap, F, of the acoustic and optical power densities.

$$\eta_{Bragg} \propto \Delta N W F$$

Using a large number of interdigital fingers gives a higher electrical to acoustical energy coupling and serves to increase index contrast. Using the fundamental mode of the waveguide ensures that we maximize the overlap integral. Finally, increasing the transducer aperture, by lengthening the fingers, increases the interaction length.

We cannot make transducers arbitrarily efficient because of a tension that arises between diffraction efficiency and transducer parameters like bandwidth and ohmic loss.

Electrical bandwidth is defined as the 3db bandwidth of the transducer's electrical

frequency response and it goes as:

$$\frac{\Delta f_{electrical}}{f_{center}} \approx \frac{1}{N}$$

(4.1)

leading us to limit the number of transducer finger pairs, N.

The Acousto-Optic Bragg bandwidth is defined as the 3db bandwidth of the diffracted light intensity and it goes as:

$$\Delta f_{Bragg} \propto \frac{1}{f_0 W}$$

Leading us to limit the length of the fingers, W.

Finally, the ohmic loss in the transducers increases with finger length, W.

$$R_{ohm} = \frac{4W R_s}{N\Lambda}$$

(4.2)

where R_s is the resistance per square, N is the number of finger pairs and Λ is the acoustic wavelength.
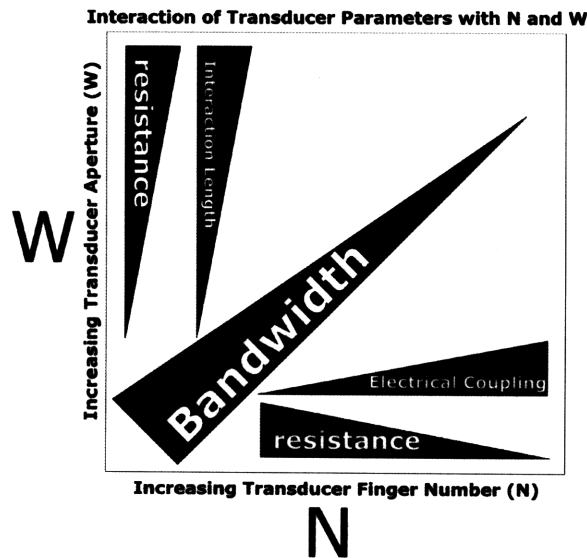

Figure 4-8: A simplified visualization of the interaction of transducer design parameters

Mode coupling efficiency goes as a function of collinear interaction length, L:

$$\eta_{modecoupling} \propto \frac{L^2}{W} P_a \qquad (4.3)$$

Where P_a is acoustic power. I want the coupling region to be as long and narrow as possible. However, this will be limited by the angular bandwidth of the system as high-angle information will be Bragg diffracted away from the center of acoustic beam (walk-off).

Resolution, or number of resolvable spots, in the system is a function of transducer bandwidths and interaction lengths W and L for horizontal and vertical respectively:

$$Res_h = \frac{W_{beam}}{v_y} \Delta f_{bragg} \qquad (4.4)$$

W_{beam} is the laser beam waist which should correspond roughly to the collinear transducer aperture and the waveguide width.

$$Res_v = \frac{L}{v_x} \Delta f_{modecoupling} \qquad (4.5)$$

Note that, horizontally, there is a small interaction length (i.e. 1mm) and a large composite Bragg bandwidth (i.e. 1GHz). Vertically the interaction length is large (i.e. 20mm) but the bandwith is small (i.e. 50Mhz). Since $v_x \approx v_y$, the vertical resolution should roughly match the horizontal resolution. This is important since the descanning scheme will require that every horizontal point is deflected to a distinct vertical level on the HOE for optimal output.

The number of spots (for $v_x \approx v_y = 3909$) is, coincidentally, a familiar one:

$$Res_h = \frac{1mm}{3909m/s} 1GHz \approx 256 spots$$

This number would ostensibly serve as an upper limit for views in the final display.

4.2.3 Parameter choice and transducer placement

The device length is 35mm and the maximum interaction length for diffracted light is 30mm. I want each diffracted beam to have at least 10mm of interaction so I am left with 20mm of space for all the Bragg diffracting transducers. I have chosen to use 10 transducers so I have roughly 2mm of linear space for each transducer and this gives me an upper bound on W. I want my 10 transducers to give me a composite bandwidth of at least 1Ghz which puts an upper bound[2] on N. Now each transducer will have to be rotated so that the illumination beam enters the transducer's acoustic wavefront at the Bragg angle for that transducer. The illumination angle is fixed so each of the transducer's angles will vary. I've chosen the illumination angle to correspond to twice the Bragg angle of the center tranducer (see Fig 4-9) so that the composite output will center around the output of the middle transducer. I've also chosen to order the transducers from high to low frequency (moving towards the illumination) so that the fan of diffracted output beams creates a real focus. The real focus scheme, as opposed to the virtual focus scheme, results in less beam walk-off for the collinear, mode-conversion interaction.

---

[2] I only have an upper bound on N if I have the same number of fingers for each transducer. It might be more optimal to have a varying number of transducers, but I've kept them the same so that I can more easily compare the behavior of the transducers from one center frequency to the next.
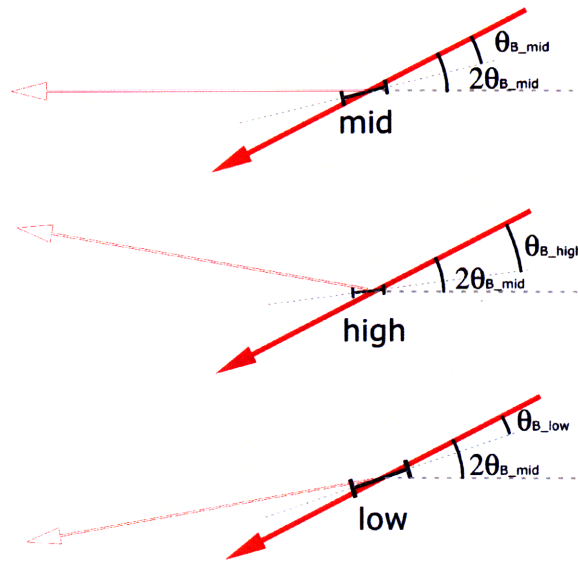
Figure 4-9: The illumination light (solid arrow) is incident at twice the Bragg angle of the middle transducer so that the diffracted light will be aimed straight along the optical axis. The anglular placement of the higher and lower frequency transducers are biased by the Bragg angle of the middle transducer so that their combined diffracted outputs will create a fan of light centered around the output of the middle transducer.
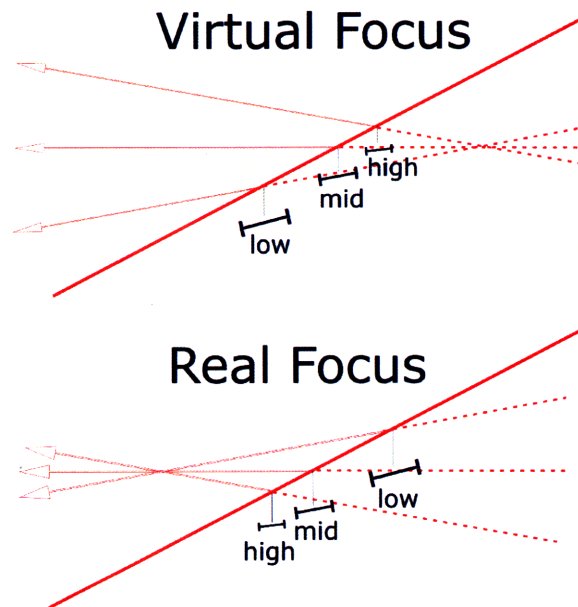

Figure 4-10: The transducers can be ordered from low to high or from high to low frequency. I chose high to low because this arrangement creates a real focus which reduces the amount of beam walk-off in the collinear interaction

4.3 Design Summary

The following tables give a basic summary of the design parameters of the guided wave scanner. They are by no means optimal, but they do not grossly violate any of the restrictions placed by the considerations given in the previous section.
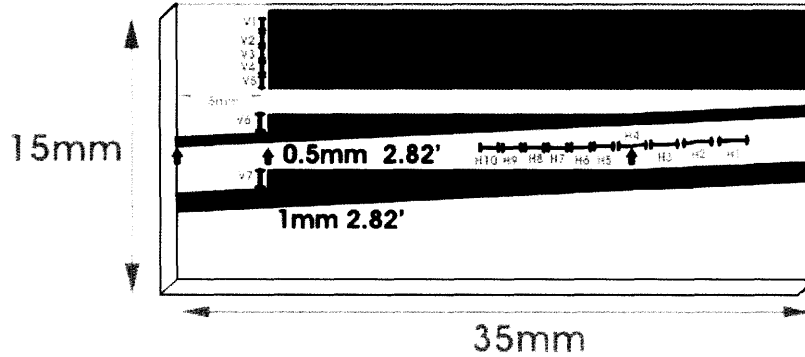

Figure 4-11: Waveguide and transducer layout. Notice that there are extra transducers and waveguides above and below the central waveguide that serve as test structures.

Table 4.1: Waveguide Design Parameters

Type	depth	W	L	Bragg
Annealed PE	$1\mu m$	1mm	35/30mm	2.62°

Table 4.2: Transducer Design Parameters

name L/C	f_0	line	W	N	BW	Bragg
H1	250Mhz	3.9 μm	1.5mm	5	50Mhz	2.32°
H2	350Mhz	2.8 μm	1.5mm	5	70Mhz	2.12°
H3	450Mhz	2.2 μm	1.5mm	5	90Mhz	1.92°
H4	550Mhz	1.8 μm	1.5mm	5	110Mhz	1.71°
H5	650Mhz	1.5 μm	1.5mm	5	130Mhz	1.51°
H6	750Mhz	1.3 μm	1.5mm	5	150Mhz	1.31°
H7	850Mhz	1.2 μm	1.0mm	5	170Mhz	1.11°
H8	950Mhz	1.0 μm	1.0mm	5	190Mhz	0.91°
H9	1050Mhz	0.9 μm	1.0mm	5	210Mhz	0.71°
H10	1150Mhz	0.85μm	1.0mm	5	230Mhz	0.5°
V1	460Mhz	2.1 μm	0.5mm	10	46Mhz	–

Chapter 5

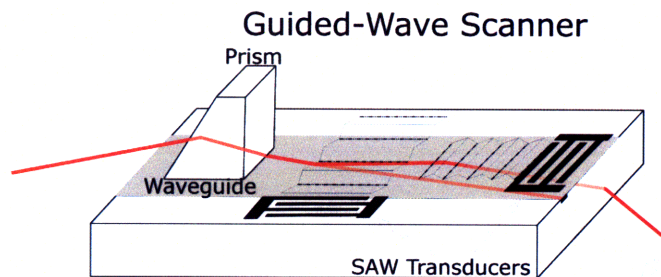# Fabrication of the Guided-Wave Scanner

Figure 5-1: 2D Scanner

The fabrication of the guided-wave scanner involves four steps: making the mask, forming the waveguide, patterning the transducers and matching the device impedance to the drive impedance.
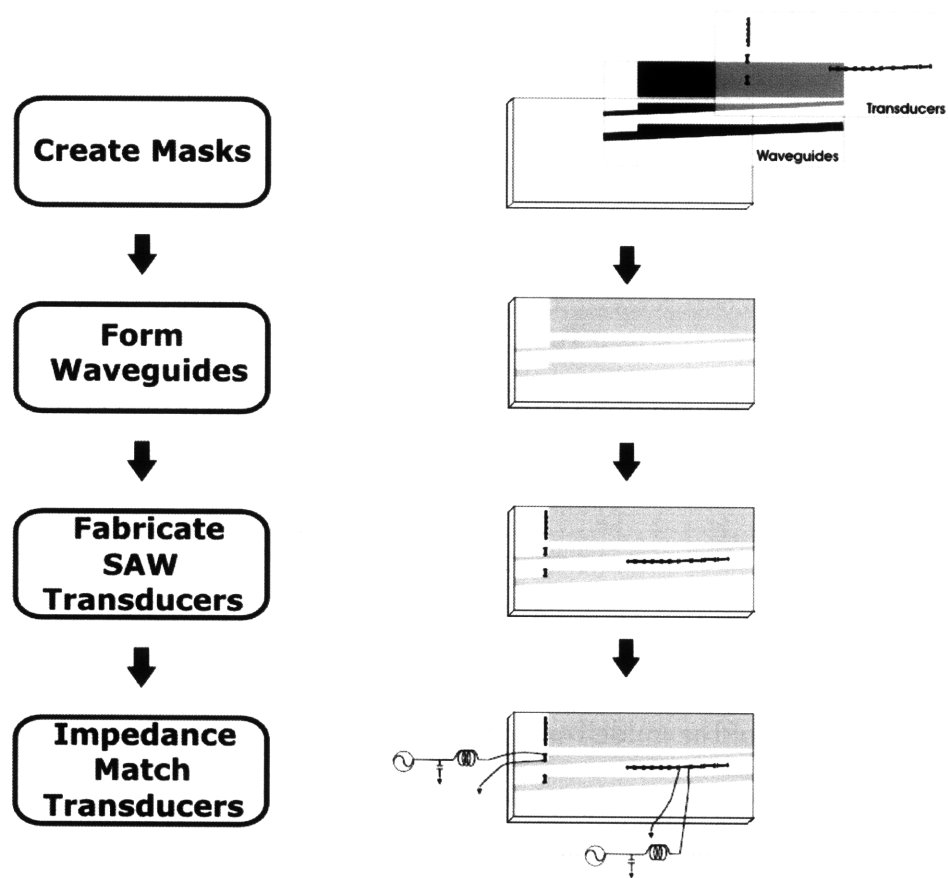
Fabricating a Guided Wave Scanner

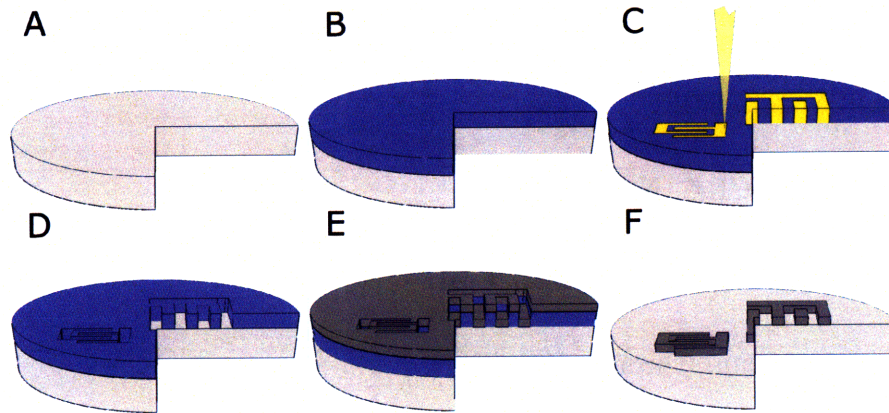Figure 5-2: Scanner Fabrication Steps

5.1 Mask Making

Figure 5-3: Mask Making Steps (A) Start with a blank fused-silica wafer (B) Spin 300nm PMMA (C) Ebeam write the transducer pattern (D) Develop exposed pattern in IPA:MIBK (E) Deposit Chromium (F) Lift-off PMMA in Acetone

For the purposes of this research, it makes more sense to use a contact mask for patterning transducers. The alternative would be to use a stepper mask, but to have such a mask made at the resolution we require (0.8μm) would be too expensive, especially when it is likely that we will only use the mask a few times before modifying the transducer design. Furthermore, contact masks can give better resolution than even stepper masks when there is a conformal contact between the mask and the Lithium Niobate substrate. The mask pattern used for fabricating guided-wave scanners is shown in Figure 5-4.

The process flow for the fabrication of a contact flex mask is given below. All of the fabrication steps were performed at either the MIT Media Laboratory, Nanostructures Laboratory (NSL), Scanning Electron Beam Laboratory (SEBL) or in the Experimental Materials Laboratory (EML) of the Microsystems Technology Laboratory (MTL).

Process Flow

Start with a clean Fused-Silica or Quartz wafer, 200-300nm thick, 3in (76mm) diameter. (Mark Optics Inc., Santa Ana, CA)

1. Spin 3.5% PMMA at 3000 RPM, NSL/EML

2. Bake on a hotplate for 2min at 150°C, NSL/EML

3. Deposit 8nm Chrome, NSL/EML

4. Ebeam Write, SEBL

5. Etch Chrome CR-7, NSL/EML

6. Develop in 2:1,IPA:MIBK, NSL/EML

7. Evaporate 150nm Chrome, NSL/EML

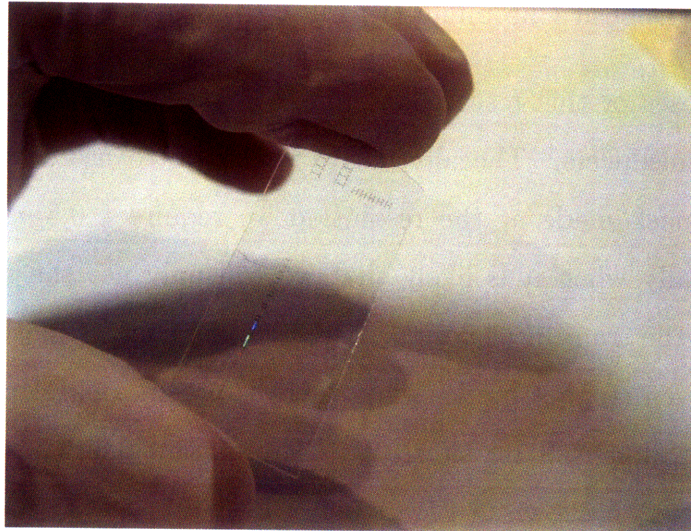8. Lift-off Chrome in Acetone or Chlorobenzene NSL/EML

Figure 5-4: transducer mask

5.2 Waveguide Fabrication

Below is the process flow for the fabricating light guides on the surface of a Lithium Niobate substrate.

Beginning substrate: Z-cut Double-Side Polished Lithium Niobate, 1mm thick (least expensive), 3in (76mm) diameter. (Crystal Technology, Palo Alto, CA)
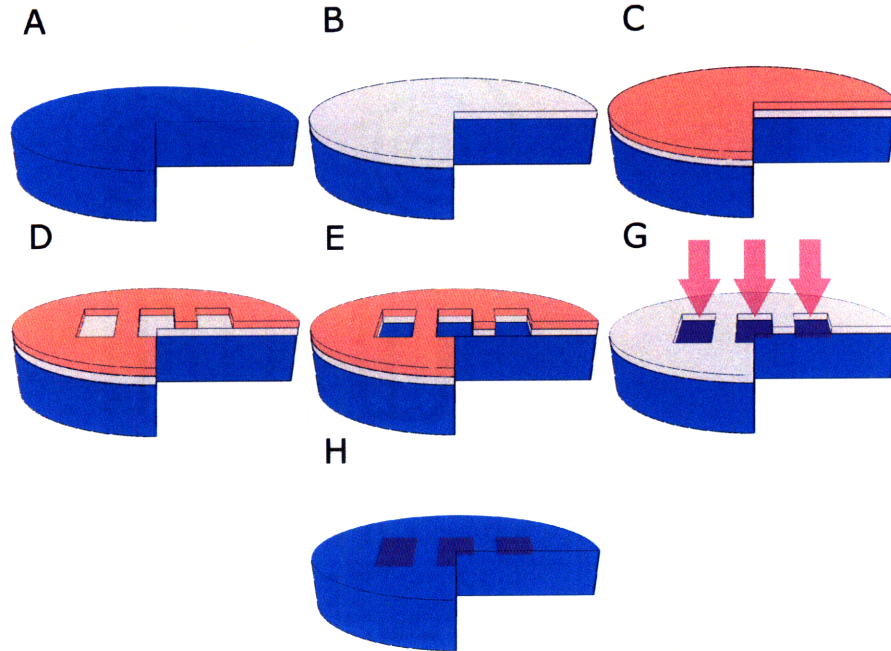
1. PECVD 250nm SiO_2, EML

Figure 5-5: Waveguide Fabrication Steps (A) Start with a clean, Z-cut Lithium Niobate wafer (B) PECVD 200nm of Silicon Oxide (C) Spin a layer of negative resist (D) Pattern the resist (E) Etch the Silicon Oxide (F) Perform Proton Exchange (G) Remove the remaining resist and oxide with Acetone and HF respectively.

2. Spin negative photoresist (Futurrex NR8-1000P), bake 15min at 100°C, NSL

3. Expose UV source to an energy of 40mJ, NSL

4. Develop in 2% R2 developer, NSL

5. Buffered Oxide Etch 1min, solvent clean, NSL

6. Proton Exchange, Benzoic Acid, Acid hood 200°(time is variable)

7. Buffered Oxide Etch, Acid Hood, NSL

5.2.1 Waveguide Analysis

Before proceeding with the fabrication of transducers, it is important to verify that a waveguide exists and that it extends to a depth exceeding 1μm. This verification is performed by prism coupling.
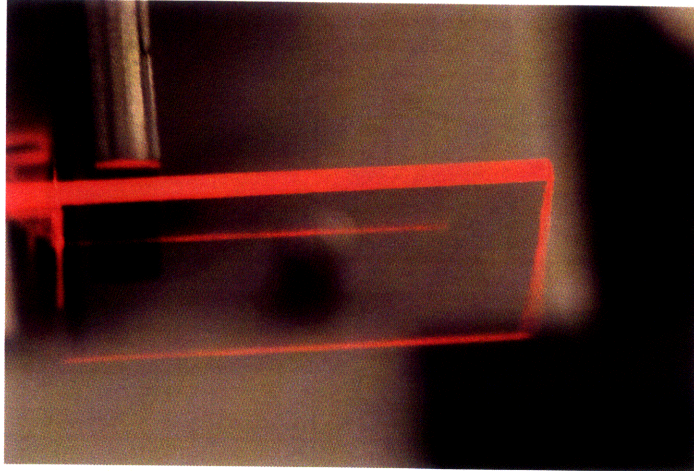
Figure 5-6: 1db/cm Loss Waveguide

5.3 Patterning Transducers

Once the waveguide is in place, transducers can be patterned on the wafer.
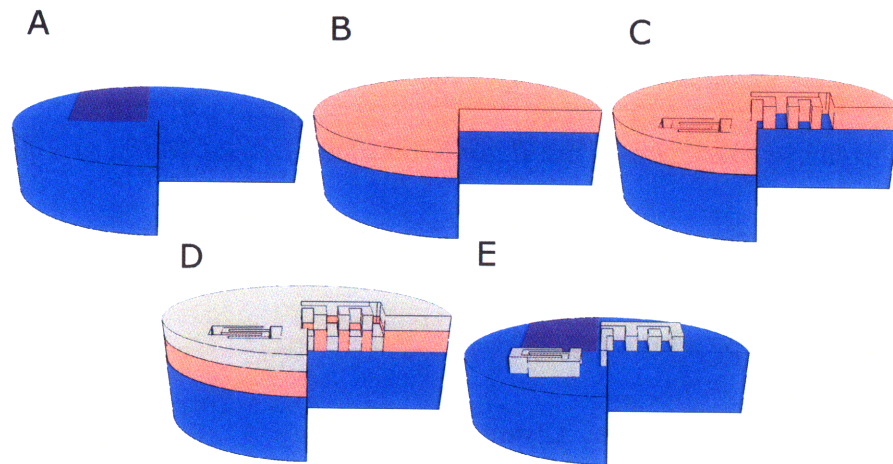

Figure 5-7: Transducer Fabrication Steps (A) Start with Proton Exchanged Lithium Niobate (B) Spin Negative Resist (C) Use flex mask to pattern resist (D) Deposit Aluminum (E) Liftoff resist with Acetone

start with Lithium Niobate wafer (Z-cut):

1. HMDS 1min/spin 1min/ air-out 1min, NSL

2. Spin (NR8-1000P) resist 3-4krpm, NSL

3. Bake at 100°C for 15min, NSL

4. Expose with i-line using a vacuum chuck, NSL

5. Develop in R2 developer for 2min (usually 1:45min clear time), rinse w/water, NSL

6. Ebeam deposit 200nm Aluminum, NSL/EML

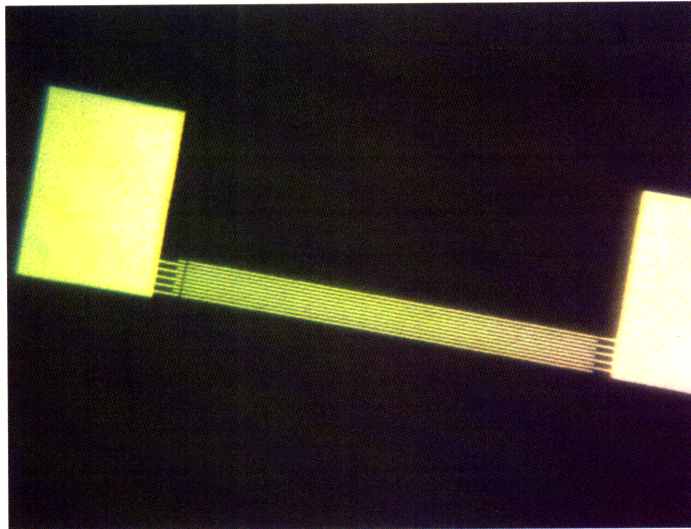7. Lift-off in Acetone (soak 15min, sonic clean for 10sec), NSL

Figure 5-8: A simple Aluminum transducer fabricated atop a Lithium Niobate substrate

5.4 Packaging

5.4.1 Diesaw

The finished wafer is cut on the diesaw. Photoresist might be used at this step to protect the smaller features from debris that may be circulating over the wafer during cutting.

5.4.2 Polishing

It is important to polish the edge of the wafer that serves as the output face for the scanned beam. Polishing down to $1\mu m$ grit gives a good surface.

5.4.3 Mounting and Wirebonding

Each die is mounted on a glass slide and sits straddled by two semicircular pcb boards with radial striplines leading to SMA connectors. The die needs to sit on a flat surface because a prism will later be clamped onto the device for testing and any bumps underneath the die may cause fractures. The width of the striplines are computed to have a 50Ω impedance.
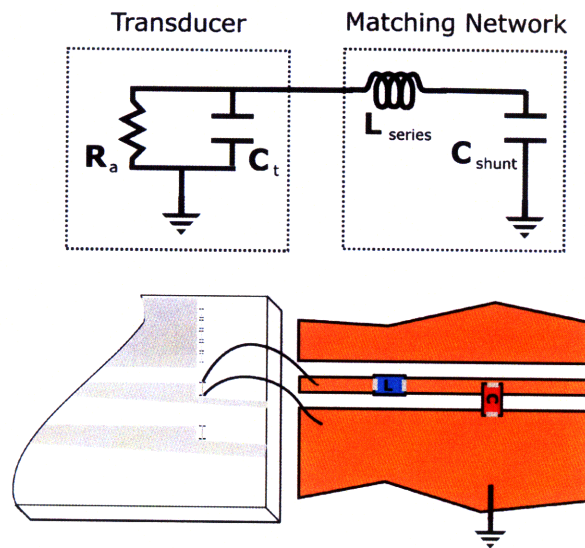
5.5 Impedance Matching

Figure 5-9: Impedance matching a device

In order to achieve maximum power transfer to the device and to minimize RF radiation into the air, it is necessary to match the device impedance to the drive impedance. Matching is done with the help of a network analyzer and a Smith chart like the one shown in Fig. **??**. The guided-wave scanner's transducers are impedance matched to 50Ω. For transducers designed to have a real impedance of 50Ω, the complex reactance can be eliminated by using a single lumped-element inductor. All other transducers can be matched with an 'L' network made of one series inductor and one shunt capacitor. The L network has its own resonance peak and it may reduce the bandwidth of the transducer. Once the devices are more fully characterized, all

future transducers will be designed to have a real impedance of 50Ω.

At frequencies above a 1 GHz, the quasi-static region is tens of centimeters and as a result care must be taken to account for the length of the cables leading from the network analyzer to the device under test.
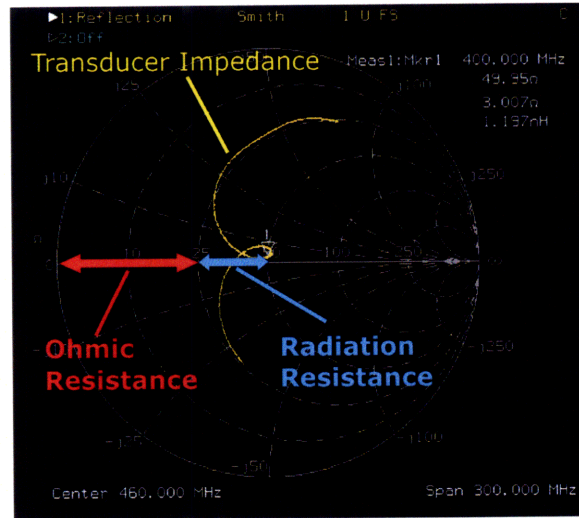

Figure 5-10: This figure shows the network analyzer's Smith chart output for the second horizontal transducer, H2. The transducer's impedance is shown looping near 50Ω. The ohmic resistance corresponds to the ohmic loss of the device. The radiation resistance corresponds to the proportion of the electrical power that is converted to acoustic waves and radiated away from the transducer. Notice that the radiation resistance is greatest near the center frequency of the transducer.

5.6   Finished Device

The finished device has 12 ports: 10 horizontal inputs, 1 vertical input and 1 vertical output. The output port is not strictly necessary to the function of the scanner but it helps sink acoustic energy that would otherwise turn into heat and makes it easy to monitor the SAW signal while the device is operating.
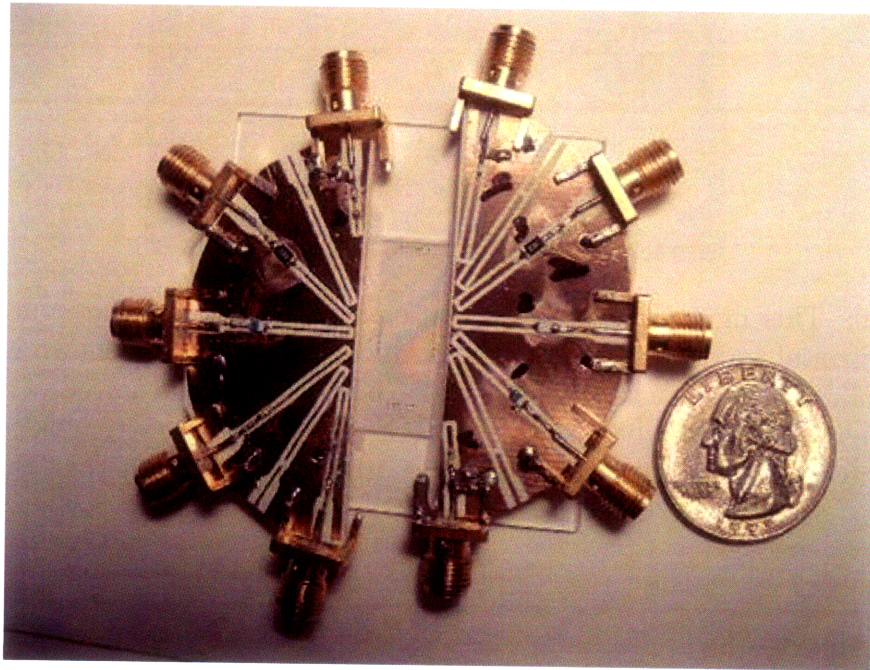
Figure 5-11: Packaged Device

Chapter 6

Summary of Results

The guided-wave scanner has successfully demonstrated coupling, confinement, SAW generation, Bragg diffraction and mode-conversion. A waveguide was fabricated with a loss approaching 1dB. Seven of the horizontal transducers where correctly patterned during fabrication and five demonstrated target electrical bandwidths for a total bandwidth in excess of 500Mhz. High diffraction efficiency of 20% was observed for Bragg diffraction on one horizontal transducer when tested optically. Cascaded horizontal and vertical deflections were demonstrated. An unanticipated mode-coupling region was identified at 530MHz and, efficient mode coupling observed which met the target bandwidth of 50MHz.

6.1 Waveguide Results

Parameter	Design Goal	Experiment	Explanations/Notes
Waveguide Loss	1db	1db	Good result, seems reproducible
Coupling Frequency	460 MHz	510-530 MHz	Difference due to anneal?
Coupling Efficiency	Good	Good	
Coupling Bandwidth	60MHz	60MHz	
K restoration	Good	Good	

Table 6.1: Waveguide Results

Fabricating, consistently, low-loss waveguides turned out to be the most time consuming part of this thesis work. A relatively small change in proton exchange pa-

rameters can result in a relatively large difference in waveguide loss. My experience was that longer exchanges worked better that shorter ones for waveguide loss (see Fig.6-4). This may be because deeper waveguides do a better job at confining the optical energy and in particular, keeping more light from the surface of the waveguide where there might be scattering defects. Annealing, in general, did not reduce loss and in some cases, it increased loss (this is consistent with some reports in the literature). The best results seemed to be for a 90min exchange time at 200°C with an anneal at 300°C for 45 minutes. Annealing, in the best samples, did not seem to increase loss. Temperature may have played a role, but my proton exchange setup was not sophisticated enough to allow for careful control and precise measurement of temperature within the exchange vessel itself.
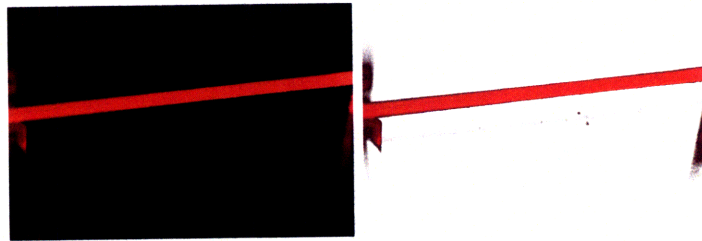

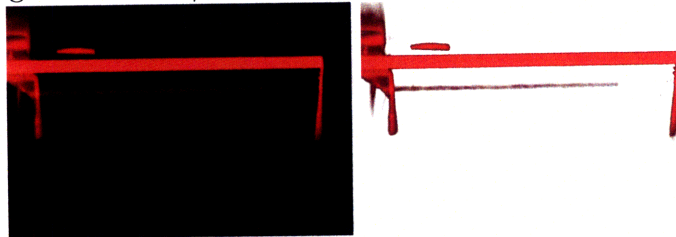Figure 6-1: 1db/cm loss waveguide with black removed

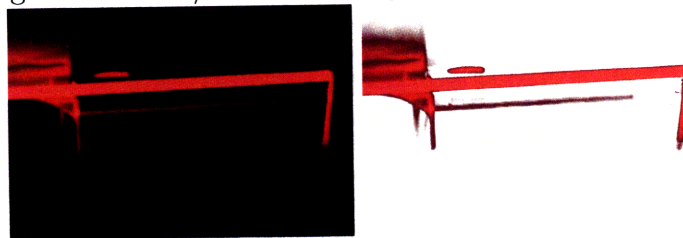Figure 6-2: 2db/cm loss waveguide with black removed

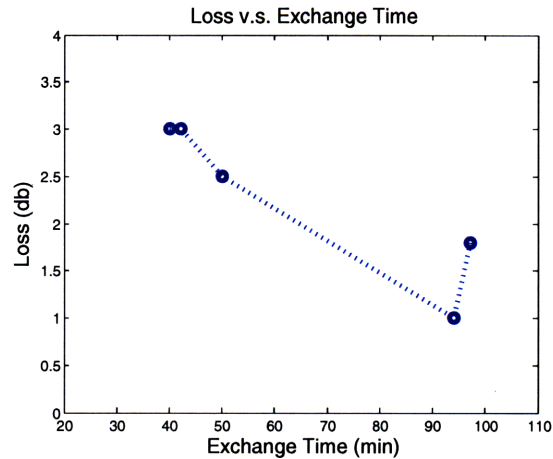Figure 6-3: 3db/cm loss waveguide with black removed

Figure 6-4: Waveguide loss versus exchange time for five samples. Exchange melt compositions were identical for all samples but temperature between samples may have varied as much as 10%

6.2 Mode-Coupling Results

The mode coupling spectrum for the waveguide is shown in Fig. 6-5. There was some response near 460MHz as expected, but there was also a wide-band response at 530MHz. This response appeared to be stronger, at least for a small set of test transducers[1], than the peak at 420MHz so vertical deflection tests were performed at the 530MHz peak (using a test transducer at 520MHz, which was the closest available).

The mode coupling demonstrated good response over a band of at least 50MHz, meeting easily the target bandwidth for vertical deflection.

Note that, in all the optical tests reported here, the beam was shaped for optimal coupling into the crystal which means the beam waist was small, some fraction of a millimeter, and was not completely collimated since it was focused at the entrance of the waveguide. These two factors may have led to some spot spreading at the output which may explain why the diffracted spots are not sharper.

---

[1]The reduced response of the 430MHz peak may have been a function of the test transducer's response so an additional test with more transducers will have to be done to confirm that 420MHz is not a better region of response.
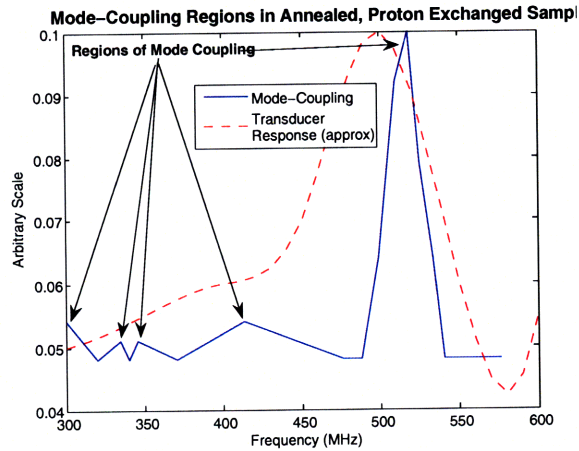
71

Figure 6-5: This figure shows the mode coupling response for transducer with a peak response near 500MHz. Mode coupling occurs at 420MHz which is not surprising (I was expecting it to be somewhere between 420 and 460MHz), but it also occurs strongly near 530Mhz and then at other regions near the tail of the transducer's frequency response (e.g. between 300 and 350MHz).
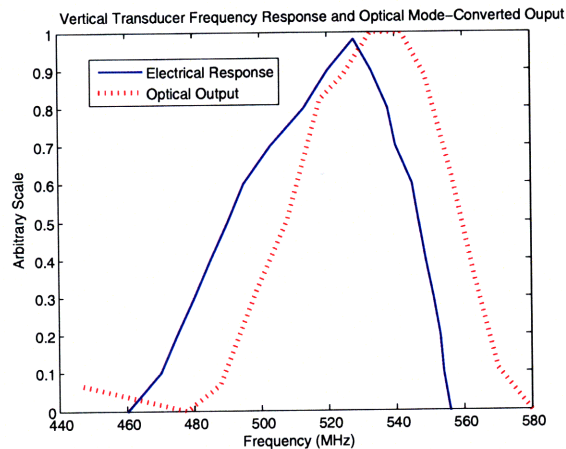

Figure 6-6: This figure shows the electrical frequency response of the vertical, mode-coupling, transducer with respect to the light output. Notice that the one tracks the other, but they are offset slightly suggesting that the vertical transducer might give greater optical output if its center frequency were a little higher.
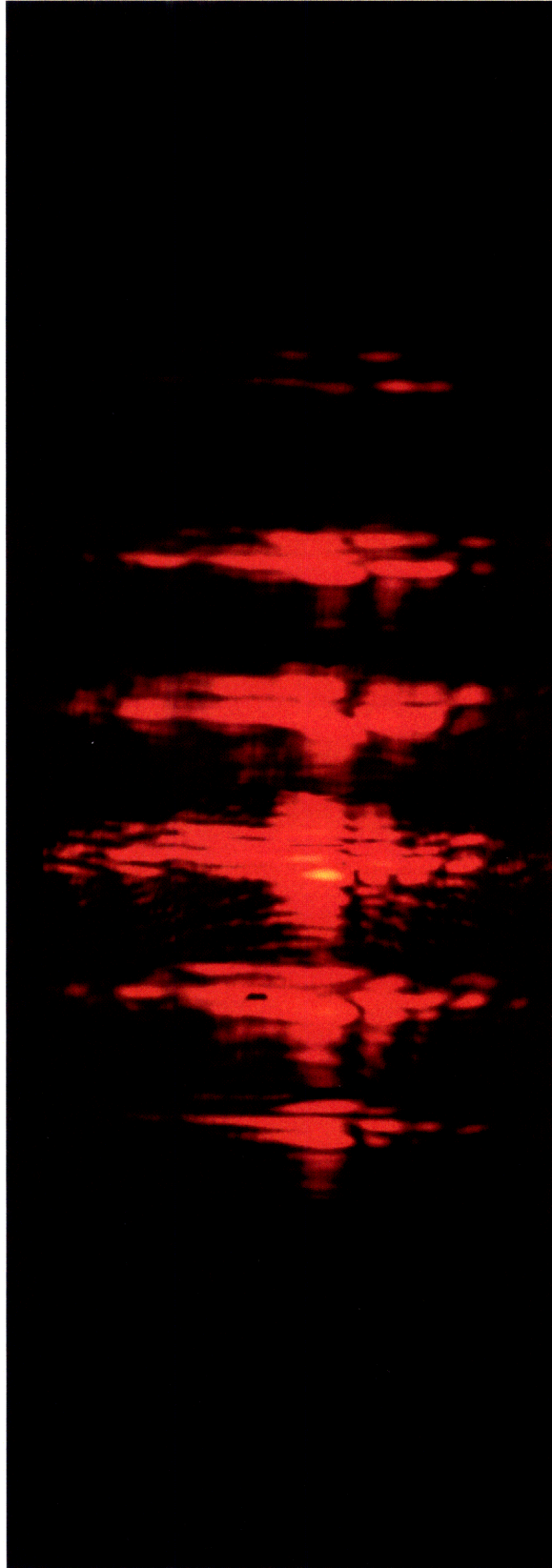
Figure 6-7: Vertical scan (composite image)

6.3 Bragg Diffraction Results

Patterning long transducers with feature sizes below $1\mu m$ proved difficult, due to diffraction spreading under the mask. A thinner resist may have to be used to obtain good results for the three transducers with the smallest features. It may also be possible to achieve smaller features by carefully optimizing exposure and development of the resist. Of the seven transducers that were patterned correctly, five showed promising electrical responses. The other two were damaged and appeared as shorts. The center frequency and bandwidth information was obtained from SWR measurements taken on a Network Analyzer. The center frequency for the transducers is shown to be different than the design frequency by as much as 50MHz in some cases. This is somewhat objective since the peak response of the transducer is affected by the output of the matching circuitry. Furthermore, a transducer's peak response will shift from the center frequency as the number of finger pairs is increased. It is easy enough to take the current data and modify the next mask to recenter the transducer's output. No explanation is offered, at this time, for why the bandwidths also seem to be much larger than the design values. The composite bandwidths are shown in Fig. 6-7 to exceed a total of 500MHz. Two transducers were damaged during testing, but three survived to have their optical output recorded and shown in fig. 6-9. The diffraction efficieny of transducer H2 was recorded and shown to be 20% at a RF drive power of 400mW.

Transducer	H1	H2	H3	H4	H5	H6	V1
Design Center Frequency (MHz)	250	350	450	550	650	750	520^2
Actual Center Frequency (MHz)	280	400	500	600	700	–	520^3
Design Bandwidth (MHz)	50	70	90	110	130	150	170
Actual Bandwidth (MHz)	50	120	180	210	160	–	50
Diffraction Efficiency (%)	–	20	–	–	–	–	–

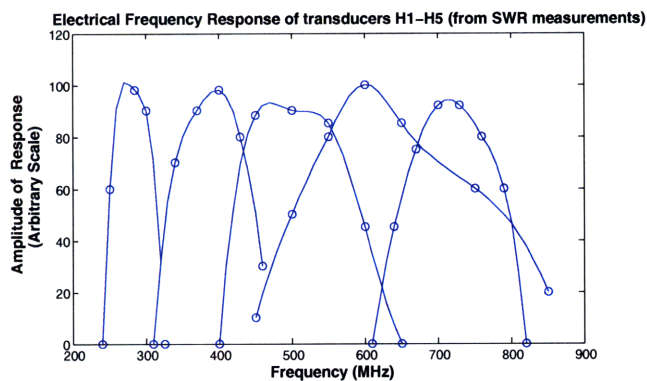Table 6.2: Horizontal Diffraction Transducer Parameters

Figure 6-8: This figure shows the electrical frequency response of the horizontal, Bragg-diffracting transducers. Notice that bandwidth per transducer goes up with center frequency and that the composite bandwith for five transducers is near 500Mhz (The 3dB level lies at 50 on this graph)
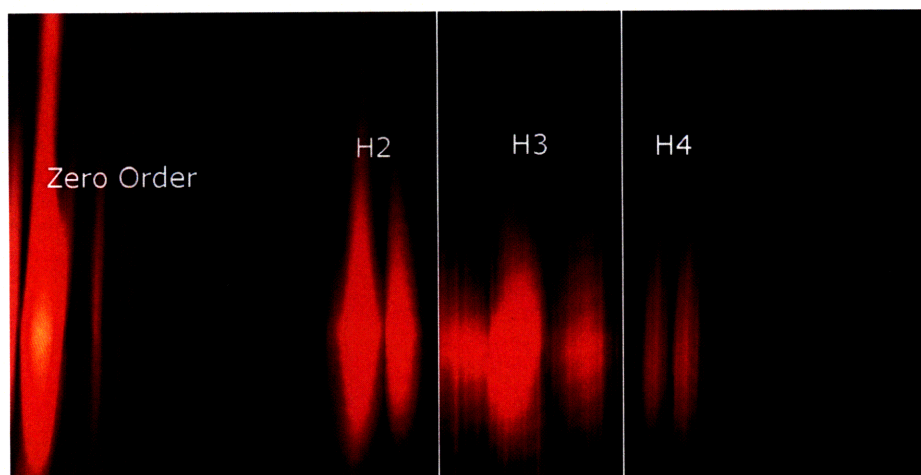

Figure 6-9: Horizontal scan output for transducers H2,H3 and H4. The sections separated by the white lines were recorded at different times and their relative positions are approximate.(Composite Image)

6.4   2D Scanning Results

A single horizontal transducer, H1, was used in conjunction with the vertical deflection to demonstrate 2D scanning (the current test setup allows for only two transducers to be driven at a time). The resulting composite image is shown in fig. 6-10.
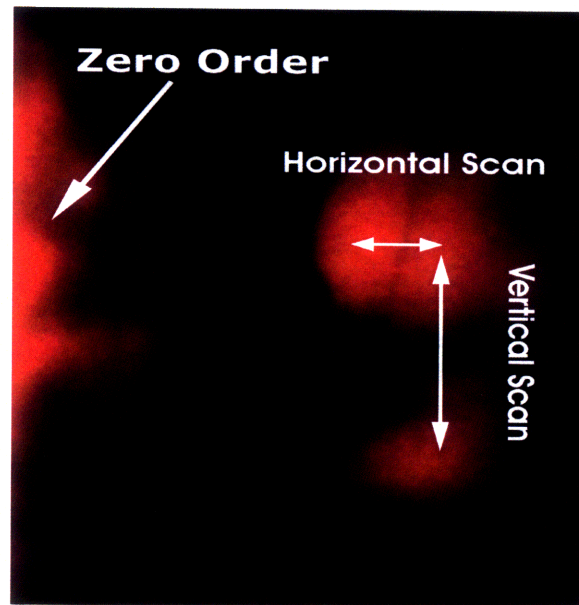

Figure 6-10: Cascaded horizontal and vertical output of the 2D Scanner using the first horizontal transducer, H1.(Composite Image)

Chapter 7

Conclusion/Future Work

7.1 What I've done

I have fabricated a device capable of demonstrating all the underlying phenomena key to the operation of a guided-wave scanner: coupling, confinement, SAW generation, Bragg diffraction and mode-conversion (both independantly and in cascade). I've been able to consistently create Annealed, Proton Exchanged waveguides with loss approaching 1db/cm. I have achieved and exceeded the target electrical and optical bandwidth in the first five transducers. I've identified a mode-coupling region at 530MHz with a relatively wide band and good efficiency that I had not anticipated.

The scanner is fit for use in the Mark III display in proportion to the degree that it meets the design specifications. Having only a fraction of the horizontal transducers working means a reduction in the display's viewing angle. The availability of sufficient vertical bandwidth means that the descanning should function as expected. The only other considerations are the power and wavelength of the illumination light. Currently the scanner's light output is on the order of micro-Watts but will likely need to be at least a few milli-Watts for a sufficiently bright display output (the Mark II uses <5mW of diffracted light). A 100mW green laser will replace the current 10mW red laser to provide the necessary optical power. Because the wavenumbers of the guided modes will change for green illumination, the current scanner's vertical deflection transducer will have to have be modified to achieve mode coupling in a green light

system.

7.2 Contributions

The scanners produced by this research are, to my knowledge, the first application of guided-wave acoustooptics to macro-scale projection and display. Additionally, the concept of using a SAW-driven vertical scan coupled with an HOE for continous optical de-rotation is also a unique contribution in the field of scanned aperture electro-holography. These two innovations effectively remove the scaling barrier that limited earlier generations of the MIT holovideo display.

7.3 Future work

7.3.1 Short-Term

The design goals for the scanner, set out at the beginning of this thesis were:

- 1 Ghz RF transducer bandwidth (which corresponds spatially to holographic resolution of 1000 lines/mm)

- 10% or greater diffraction efficiency

- aperture of 1mm or greater

Using the first five transducers, roughly half the target bandwidth was achieved. The second horizontal transducer showed 20% diffraction efficiency at the modest drive power of 400mW. It seems reasonable to expect that the other transducers should be able to function with similar efficiency, or be made to do so by tweaking aperture and input power parameters. The device was made to support a beam apertures as wide as 1mm but smaller apertures were used in practice to ease testing. Some beam shaping of the input light will need to be done for this design goal to be completed.

7.3.2 Long-Term

The guided wave scanner described in this work would improve the output and reduce the cost of many, if not most, of the 3D display designs currently being developed with more expensive, lower bandwidth modulators. It would be interesting to explore whether the scanner could be made sufficiently modular (a modular modulator!) so that it could be wildly distributed and included in a variety of 3D geometries.

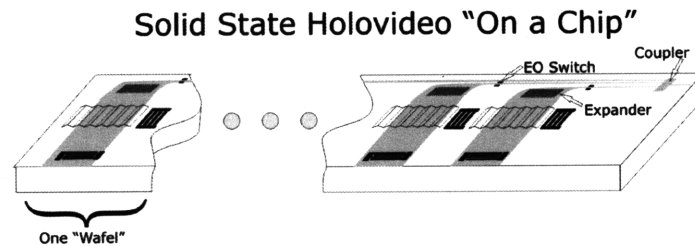**Solid State Holovideo "On a Chip"**

Figure 7-1: This is a possible instantiation of solid-state holographic video on a chip. Light travelling through waveguides would strobe holographic wavefront elements, stacked horizontally like pixels. The strobing would make descanning unnecessary but would also require that the modulator be roughly as wide as the display output.

7.3.3 Holovideo on a Chip

The MIT scanned-AOM architecture for holovideo is made of lenses, mirrors and scanning elements. During the past two decades, researchers in the field of integrated optics have been able to fabricate lenses, mirrors and scanning elements as part of waveguide systems on the surface of Lithium Niobate. It is conceivable, therefore, that we could eventually 'pull' all of holovideo's optics, with the possible exception of the output lens, onto an optical chip (see Fig. 7-1).

7.4 Concluding Statement

The work reported in this thesis has demonstrated a two-dimensional scanner capable of all the basic functions necessary to serve as part of MIT's third generation holographic video display and possibly as a building block for advanced displays in the future.

APPENDIX

Appendix A

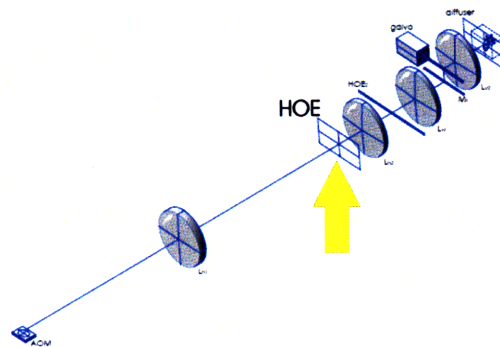# The Descan HOE

Mark III Holovideo System

Figure A-1: Location of the HOE

The descan HOE is under continued development by Quinn Smithwick, myself and Dr. Bove. This section briefly explains the basic principles of operation and describes our current method of fabrication.

A-1 HOE Function

The derotation mirrors in Mark II scan right and left in time like the mirror segments shown in Fig. A-2. If we stacked these segments on top of one another we get a helical mirror which behaves in the y like the derotation mirrors behave in time. So moving a beam vertically on this mirror causes the reflected beam to scan left and

right, but now we accomplish the scan without using moving mirrors.
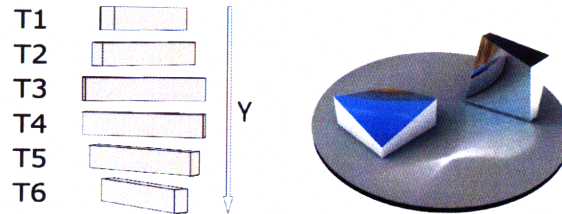
Helical Mirror

Figure A-2: A helical mirror can be thought of as a stack of long mirrors, each rotated at a slightly greater angle. Each of these mirrors represents a scanning mirror frozen at a different time, so that moving a beam vertically up and down the mirror is, in an HPO (Horizontal Parallax Only) system, the same as reflecting a beam of a single mirror that is rotating (rendering by Quinn Smithwick).

The diffraction analogue of the helical mirror is the descan HOE. Light entering the HOE at the top will be deflected horizontally at a different angle than light than light that enters the HOE near the bottom (see Fig. A-3).
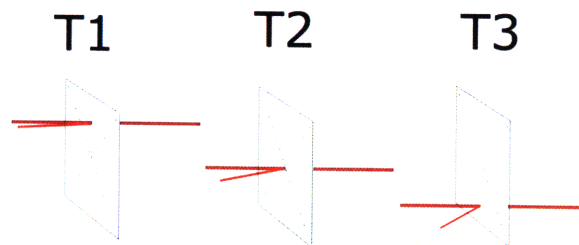

Figure A-3: Function of the HOE–light will diffract at a larger angle when passing through the bottom of the HOE than the top.

A-2 HOE Design

The HOE starts with a grating of one spatial frequency in the horizontal direction and then slowly decreases its frequency vertically. The vertical information is removed from the pattern by convolution with a sinc function which corresponds to a horizontal aperture at the fourier plane (see Fig. A-4). This means that the pattern has to be grayscale, so one must use grayscale techniques to create the HOE.
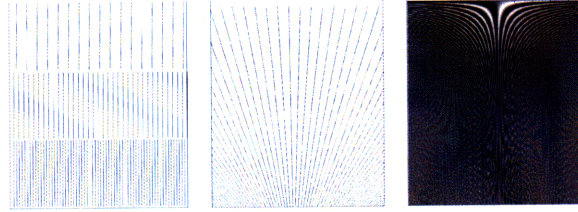
Figure A-4: The first, discretized, grating is unacceptable because the more discrete steps that are used to approximate a smooth scan, the more vertical spreading occurs as a result of diffraction. The second, slanted line, grating is also unacceptable because it has diffraction information in the vertical direction. The ideal HOE would have to be similar to the first or second grating but would use grayscale information to correct the vertical diffraction (grayscale grating courtesy of Quinn Smithwick)

A-3 HOE Fabrication

The HOE is fabricated in a manner similar to the masks used for the Guided-Wave Scanner except that the PMMA is pattern is not binary, but instead, has several discrete levels (we are currently fabricating samples with 8 levels). To achieve multiple levels in PMMA we must vary the ebeam dose during the ebeam write step. The steps can be smoothed out, if desired, by heating the HOE to get the PMMA to reflow as illustrated in Fig. A-8. Fast writespeeds can be obtained by writing with a 10keV tension since more energy is imparted to the PMMA as shown in Fig. A-7.
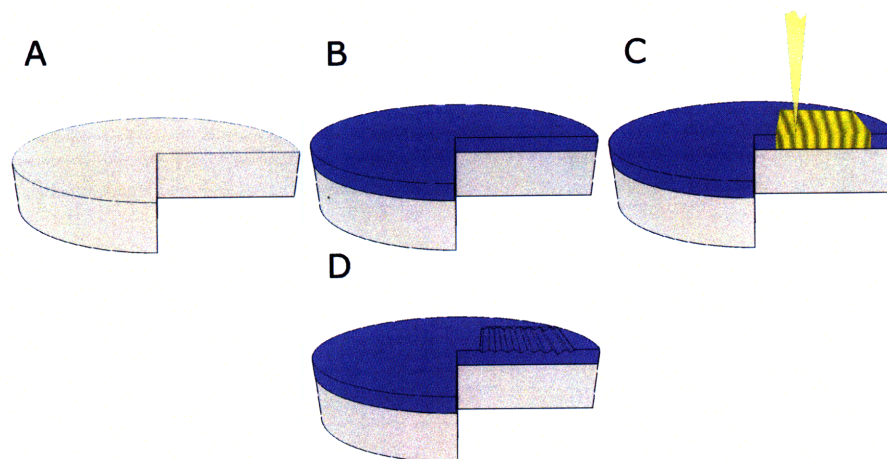

Figure A-5: HOE Fabrication Steps (A) Start with a blank fused-silica wafer (B) Spin 300nm PMMA (C) Ebeam write (with varying dose) the HOE pattern (D) Develop exposed pattern in IPA:MIBK

Figure A-6: Here are squares written at different depths in PMMA using an ebeam at 30keV and varying doses.
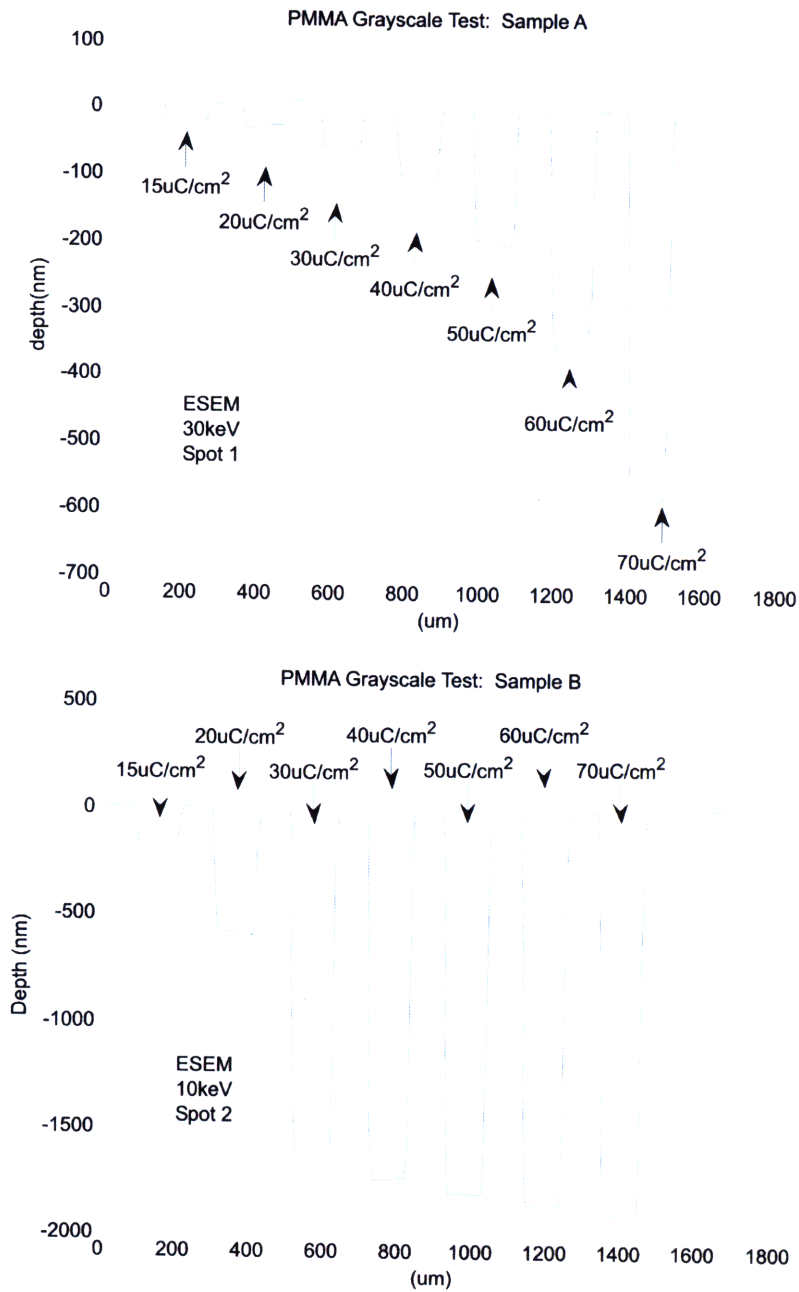

Figure A-7: Both samples above where written with the same ebeam dose the differing depths result from the fact that more energy was imparted to the film in the 10keV case.
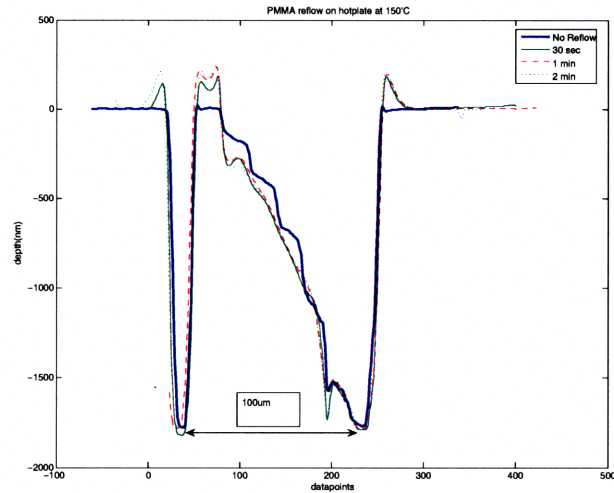
Figure A-8: It is possible to smooth out the steps in the pattern by putting the HOE in the oven and letting the PMMA reflow. Notice that heat causes the PMMA to expand and pucker in sections that have not been exposed. This can be avoided my making sure that all parts of the HOE have been exposed, at least a small amount. We do this by choosing our first level to be at a non-zero dose.

A-4 HOE Results

We have fabricated working HOEs, by other methods (direct holographic recording and fringe writing), with approximately 10% diffraction efficiency, . We aim to produce gratings with higher efficiency (30% or more) with the fabrication method described above by optimizing the PMMA thickness.

The results of our current effort and a more detailed description of the HOEs design will be given in a separate publication.

Bibliography

[1] Stephen A Benton and V. Michael Bove Jr. *Holographic Imaging*, chapter 6. Wiley-Interscience, 2008.

[2] Colin K. Campbell. *Surface Acoustic Wave Devices for Mobile and Wireless Communications*. Academic Press, 1998.

[3] Savas cedil Tay et al. An updatable holographic three-dimensional display. *Nature*, 2007.

[4] Anna Maria Matteo et. al. Collinear guided wave to leaky wave acoustooptic interactions in proton-exchanged linbo3. *IEEE Transactions on Ultrasonics, Ferroelectrics, and Frequency Control*, 47(1), 1986.

[5] Maurice Stanley et al. 3d electronic holography display system using a 100 megapixel spatial light modulator. In *Proc. of the SPIE*, number 5249, pages 297–308, 2004.

[6] W. Richard Smith et. al. Analysis of interdigital surface wave transducers by use of an equivalent circuit model. *IEEE Transactions on Microwave Theory and Techniques*, MTT-17(11), 1969.

[7] Mary Lou Jepsen. Holographic video: Design and implementation of a display system. Master's thesis, MIT, 1989.

[8] C.E. Rice J.L. Jackel and J.J. Vaselka. Proton exchange for high index waveguides in linbo3. *Applied Physics Letters*, 41, 1982.

[9] Shoji Kakio and Yasuhiko Nakagawa. Photo-elastic constants of proton-exchanged linbo$_3$. *Japanese Journal of Applied Physics Letters 34, (1995)*.

[10] Joel S. Kollin. Design and information considerations for holographic television. Master's thesis, MIT, 1988.

[11] Norbert Leister, Armin Schwerdtner, Gerald Ftterer, Jean-Christophe Olaya Steffen Buschbeck, and Stanislas Flon. Full-color interactive holographic projection system for large 3d scene reconstruction. In *Proc. of the SPIE*, number 6911, 2008.

[12] Bala Munjuluri Michael L. Huebschman and Harold R. Garner. Dynamic holographic 3-d image projection. *Optics Express*, 11(5):437–445, 2003.

[13] Mamoru Miyawaki and Shigetaro Ogura. Efficient, damage resistant linbo$_3$ acousto-optic waveguide deflector. *Applied Physics Letters 49, 16- (1986)*.

[14] Jae-Woong Moon, Dong-Whi Lee, Seung-Cheol Kim, and Eun-Soo Kim. Color lcos-based full-color electro-holographic 3d display system. cockpit and future displays for defense and security. In *Proc. of the SPIE*, number 5801, pages 294–303, 2005.

[15] DP Morgan. *Surface-Wave Devices for Signal Processing*. Elsevier, 1991.

[16] S. L. Hill R. K. Dorval O. S. Cossairt, J. Napoli and G. E. Favalora. Occlusion-capable multiview volumetric three-dimensional display. *Applied Optics*, 46.

[17] Takanori Okoshi. *Three-dimensional Imaging Techniques*. Academic Press, 1976.

[18] T. C. Poon, B. W. Schilling, M. H. Wu, K. Shinoda, and Y. Suzuki. Real-time two-dimensional holographic imaging by using an electron-beam-addressed spatial light modulator. *Opt. Lett. 18, 63- (1993)*.

[19] Proklov. Multichannel waveguide devices using collinear acoustooptic interaction. *Institute of Radio Engineering and Electronics of the Russian Academy of Sciences*, 1992.

[20] D. Smalley and Thomas Pastureau. Eigenmode method for fast cascade of p matrices takinging into account mode coupling at reflection. pending release for publication.

[21] Daniel Smalley. Integrated optics for holographic video. Master's thesis, MIT, 2006.

[22] Daniel E. Smalley, Quinn Y. J. Smithwick, and Jr. V. Michael Bove. Holographic video display based on guided-wave acousto-optic devices. In *Proc. SPIE Practical Holography XXI: Materials and Applications*, number 6488, 2007.

[23] M. Solal, V. Laude, and S. Ballandras. A p-matrix based model for saw grating waveguides taking into account modes conversion at the reflection. *IEEE Transactions on Ultrasonics, Ferroelectrics and Frequency Control*, 51(12), 2004.

[24] J. Y et al Son. Pulsed laser holograhic video. In *Proc. of the SPIE*, number 2652, pages 24–28, 1996.

[25] Pierre St.-Hilaire. *Scalable Architechtures for Holographic Video*. PhD thesis, MIT, 1988.

[26] Atsuhiko Sugita, Kunihiro Sato, Masakazu Morimoto, and Kensaku Fujii. Full-color holographic display with wide visual field and viewing zone. In *Proc. of the SPIE*, number 6016, page 60160Y, 2005.

[27] P.K. Tien and R. Ulrich. Theory of prism-film coupler and thin-film light guides. *Journal of the Optical Society of America*, 60(10), 1970.

[28] Chen Tsai. Guided-wave acousto optic two-dimensional scanner. *Fiber and Integrated Optics*, 1998.

[29] C.S. Tsai. *Guided-Wave Acousto-Optics: Interactions Devices and Applications*. Springer-Verlag, 1990.

[30] K.K. Wong. *Properties of Lithium Niobate*. Institution of Engineering and Technology, 2002.